

Algorithms and software for projections onto intersections of convex and non-convex sets with applications to inverse problems.

Bas Peters^{*}, Felix J. Herrmann[#]

^{*}Seismic Laboratory for Imaging and Modeling (SLIM), University of British Columbia

[#]Georgia Institute of Technology

Abstract

We propose algorithms and software for computing projections onto the intersection of multiple convex and non-convex constraint sets. The software package, called `SetIntersectionProjection`, is intended for the regularization of inverse problems in physical parameter estimation and image processing. The primary design criterion is working with multiple sets, which allows us to solve inverse problems with multiple pieces of prior knowledge. Our algorithms outperform the well known Dykstra’s algorithm when individual sets are not easy to project onto because we exploit similarities between constraint sets. Other design choices that make the software fast and practical to use, include recently developed automatic selection methods for auxiliary algorithm parameters, fine and coarse grained parallelism, and a multilevel acceleration scheme. We provide implementation details and examples that show how the software can be used to regularize inverse problems. Results show that we benefit from working with all available prior information and are not limited to one or two regularizers because of algorithmic, computational, or hyper-parameter selection issues.

Keywords

inverse problems, alternating direction method of multipliers, parallel computing, software, projection methods

Introduction

We consider problems of the form

$$\mathcal{P}_{\mathcal{V}}(m) \in \arg \min_x \frac{1}{2} \|x - m\|_2^2 \quad \text{subject to} \quad x \in \bigcap_{i=1}^p \mathcal{V}_i, \quad (1)$$

which is the projection of a vector $m \in \mathbb{R}^N$ onto the intersection of p convex and possibly non-convex sets \mathcal{V}_i . The projection in equation (1) is unique if all sets are closed and convex. The projection operation is a common tool used for solving constrained optimization problems of the form

$$\min_m f(m) \quad \text{subject to} \quad m \in \bigcap_{i=1}^p \mathcal{V}_i. \quad (2)$$

Examples of algorithms that use projections include spectral projected gradient descent [SPG, Birgin et al., 1999], projected quasi-Newton [Schmidt et al., 2009], and projected Newton-type methods [Bertsekas, 1982,

Schmidt et al., 2012]. In the above optimization problem, the function $f(m) : \mathbb{R}^N \rightarrow \mathbb{R}$ is at least twice differentiable and may also be non-convex. Alternatively, proximal algorithms solve

$$\min_m f(m) + \iota_{\mathcal{V}}(m), \quad (3)$$

which is equivalent to (2) and where $\iota_{\mathcal{V}}(m)$ is the indicator function of the set $\mathcal{V} \equiv \bigcap_{i=1}^p \mathcal{V}_i$, which returns zero if m is an element of the intersection and infinity otherwise. Because applications may benefit from using non-convex sets \mathcal{V}_i , we also consider those sets in the numerical examples. While we do not provide convergence guarantees for this case, we will work with some useful/practical heuristics.

The main applications of interest in this work are inverse problems for the estimation of physical (model) parameters ($m \in \mathbb{R}^N$) from observed data ($d_{\text{obs}} \in \mathbb{C}^s$). Notable examples are geophysical imaging problems with seismic waves [full-waveform inversion, see, e.g., Tarantola, 1986, Pratt et al., 1998, Virieux and Operto, 2009] for acoustic velocity estimation and direct-current resistivity problems [DC-resistivity, see, e.g., Haber, 2014] to obtain electrical conductivity information. These problems have ‘expensive’ forward operators, i.e., evaluating the objective (data-misfit) $f(m)$ requires solutions of many partial-differential-equations (PDEs) if the PDE constraints are implicit in $f(m)$, which corresponds to a reduced data-misfit [Haber et al., 2000]. In our context, each set \mathcal{V}_i describes a different type of prior information on the model m . Examples of prior knowledge as convex sets are bounds on parameter values, smoothness, matrix properties such as the nuclear norm, and whether or not the model is blocky with sharp edges (total-variation like constraints via the ℓ_1 norm). Non-convex sets that we use in the numerical examples include the annulus (minimum and maximum ℓ_2 norm), limited matrix rank, and vector cardinality.

Aside from the constrained minimization as in problem (2), we consider feasibility (also known as set-theoretic estimation) problem formulations [e.g., Youla and Webb, 1982, Trussell and Civanlar, 1984, Combettes, 1993, 1996]. Feasibility only formulations accept any point in the intersection of sets \mathcal{V}_i that describe constraints on model parameter properties, and a data-fit constraint $\mathcal{V}_p^{\text{data}}$ that ties the unknown model vector x to the observed data $d_{\text{obs}} \in \mathbb{R}^M$ via a forward operator $F \in \mathbb{R}^{M \times N}$. Examples of data-constraint sets are $\mathcal{V}^{\text{data}} = \{x \mid l \leq (Fx - d_{\text{obs}}) \leq u\}$ and $\mathcal{V}^{\text{data}} = \{x \mid \|Fx - d_{\text{obs}}\|_2 \leq \sigma\}$. The upper and lower bounds are vectors l and u and $\sigma > 0$ is a scalar that depends on the noise level. The forward operators are linear and often computationally ‘cheap’ to apply. Examples include masks and blurring kernels. In case there is a good initial guess available, we can choose to solve a projection rather than feasibility problem by adding the squared ℓ_2 distance term as follows:

$$\min_x \frac{1}{2} \|x - m\|_2^2 \quad \text{s.t.} \quad \begin{cases} x \in \mathcal{V}_p^{\text{data}} \\ x \in \bigcap_{i=1}^{p-1} \mathcal{V}_i \end{cases} . \quad (4)$$

To demonstrate the benefits of this constrained formulation, we recast joint denoising-deblurring-inpainting and image desaturation problems as (4). Especially when we have a few training examples from which we can learn constraint set parameters, the feasibility and projection approaches conveniently add many pieces of prior knowledge in the form of multiple constraint sets, but without any penalty or trade-off parameters. For instance, [Combettes and Pesquet, 2004] show that we can observe ‘good’ constraint sets, such as the average of the total variation of a few training images. We address increasing computational demand that comes with additional constraint sets with a reformulation of problem (4), such that we take into account similarity between sets, and split the problem up into simple parallel computations where possible.

Projected gradient and similar algorithms naturally split problem (2) into a projection and data-fitting part. In this setting, software for computing projections onto the intersection of sets can work together with codes for physical simulations that compute $f(m)$ and $\nabla_m f(m)$, as we show in one of the numerical examples. See `dolphin-adjoint` [Farrell et al., 2013], `Devito` [Kukreja et al., 2016, Louboutin et al., 2018] in `Python` and `WAVEFORM` [Da Silva and Herrmann, 2017], `jInv` [Ruthotto et al., 2017], and `JUDI` [Witte et al., 2018] in `Julia` for examples of recent packages.

Compared to regularization via penalty functions (that are not an indicator function), constrained problem formulations (2 and 4) have several advantages when solving physical parameter estimation problems. Penalty methods

$$\min_m f(m) + \sum_i^p \alpha_i R_i(m) \quad (5)$$

add prior knowledge through $p \geq 1$ penalty functions $R_i(m) : \mathbb{R}^N \rightarrow \mathbb{R}$ with scalar weights $\alpha_i > 0$ to the data-misfit term $f(m)$. Alternatively, we can add penalties to the objective and work with a data constraint instead—i.e., we have

$$\min_m \sum_{i=1}^p \alpha_i R_i(m) \quad \text{s.t.} \quad f(m) \leq \sigma, \quad (6)$$

generally referred to as Basis Pursuit Denoise [Mallat and Zhang, 1992, Chen et al., 2001, van den Berg and Friedlander, 2009, Aravkin et al., 2014], Morozov/residual regularization [Ivanov et al., 2013], or Occam’s inversion [Constable et al., 1987]. The scalar σ relates to the noise level in the data. For convex constraints/objectives/penalties, constrained, penalty and data-constrained problems are equivalent under certain conditions and for specific $\alpha - \sigma$ pairs [Vasin, 1970, Gander, 1980, Golub and von Matt, 1991, van den Berg and Friedlander, 2009, Aravkin et al., 2016, Tibshirani, 2017], but differ in algorithmic implementation and in their ability to handle multiple pieces of prior information ($p > 1$). In that case, the simplicity of adding penalties is negated by the challenge of selecting multiple trade-off parameters (α_i). For this, and for reasons we list below, we prefer constrained formulations that involve projections onto the intersection of constraint sets (problem 1). Constrained formulations

- **satisfy prior information at every iteration** PDE-based inverse problems require model parameters that are in an interval for which the mesh (PDE discretization) is suitable, i.e., we have to use bound constraints. Projection-based algorithms satisfy all constraints at every iteration and give the user precise control of the model properties. This allows us to start solving a non-convex inverse problem with certain constraints, followed by a solution stage with ‘looser’ constraints. [Smithyman et al., 2015, Esser et al., 2016, 2018, Peters and Herrmann, 2017, Peters et al., 2018] apply this strategy to seismic full-waveform inversion to avoid local minimizers that correspond to geologically unrealistic models.
- **require a minimum number of manual tuning parameters for multiple constraints** We want to avoid the time-consuming and possibly computationally costly procedure of manually tuning numerous nuisance parameters. Constraint sets have the advantage that their definitions are independent of all other constraint definitions. For penalty functions, the effect of the weights α_i associated with each R_i on the solutions of an inverse problem depends on all other α_i and R_i . For this reason, selecting multiple scalar weights to balance multiple penalty functions becomes increasingly difficult as we increase the number of penalties.
- **make direct use of prior knowledge** We can observe model properties from training examples and use this information directly as constraints [Combettes and Pesquet, 2004, see also numerical examples in this work]. Penalty and basis-pursuit type methods first need to translate this information into penalty functions and scalar weights.

Most classical and recently proposed methods to project onto an intersection of multiple (convex) sets, such as Dykstra’s algorithm and variants [Dykstra, 1983, Boyle and Dykstra, 1986, Censor, 2006, Bauschke and Koch, 2015, López and Raydan, 2016, Aragón Artacho and Campoy, 2018], (see also Appendix A), use projections onto each set separately, denoted as $\mathcal{P}_{V_i}(\cdot) : \mathbb{R}^n \rightarrow \mathbb{R}^n$. The projection is a black box, and this may create difficulties if the projection onto one or more sets has no known closed-form solution. We then need another iterative algorithm to solve the sub-problems. This nesting of algorithms may lead to problems with the selection of appropriate stopping criteria for the sub-problem solver. In that case, we need two sets of stopping criteria: one for Dykstra’s algorithm itself and one for the iterative algorithm that computes the

individual projections. Projections need to be sufficiently accurate such that Dykstra’s algorithm converges. At the same time, we do not want to waste computational resources by solving sub-problems more accurately than necessary. A second characteristic of the black-box projection algorithms is that they treat every set individually and do not attempt to exploit similarities between the sets. If we work with multiple constraint sets, some of the set definitions may include the same or similar linear operators in terms of sparsity (non zero) patterns.

Besides algorithms that are designed specifically to compute projections onto the intersection of multiple sets, there exist software packages capable of solving a range of generic optimization problems. However, many of the current software packages are not designed to compute projections onto intersections of multiple constraint sets where we usually do not know the projection onto each set in closed form. This happens, for instance, when the set definitions include linear operators A that satisfy the relation $AA^\top \neq \alpha I$ for $\alpha > 0$. A package such as `Convex` for Julia [Udell et al., 2014], an example of disciplined convex programming (DCP), does not handle non-convex sets and requires lots of memory even for large and sparse linear operators from problems on 2D grids. The high memory demands are a result of the packages that `Convex` can call as the back-end, for example, `SCS` [O’Donoghue et al., 2016] or `ECOS` [Domahidi et al., 2013]. These solvers work with matrices that possess a structure similar to

$$\begin{pmatrix} \star & (A_1^\top & \dots & A_p^\top) \\ \begin{pmatrix} A_1 \\ \vdots \\ A_p \end{pmatrix} & & \star & \end{pmatrix}, \quad (7)$$

This block-structured system becomes prohibitively large in case we work with multiple constraint sets that include a linear operator in their definitions. The software that comes closer to our implementation is `Epsilon` [Wytock et al., 2015], which is written in Python. Like our proposed algorithms, `Epsilon` also employs the alternating direction method of multipliers (ADMM), but reformulates optimization problems by emphasizing generalized proximal mappings as in equation (12, see below). Linear equality constraints then appear as indicator functions, which leads to different linear operators ending up in different sub-problems. Contrary, we work with a single ADMM sub-problem that includes all linear operators. The `ProxImaL` software [Heide et al., 2016] for Python is designed for linear inverse problems in imaging using ADMM with a similar problem reformulation. However, `ProxImaL` differs fundamentally since it applies regularization with a relatively small number of penalty functions. While in principle it should be possible to adapt that package to constrained problem formulations by replacing penalties with indicator functions, `ProxImaL` is in its current form not set up for that purpose. Finally there is `StructuredOptimization` [Antonello et al., 2018] in Julia. This package also targets inverse problems by smooth+non-smooth function formulations. Different from the goal of this work, `StructuredOptimization` focusses on problems with easy to compute generalized proximal mappings (12), i.e., penalty functions or constraints that are composed with linear operators that satisfy $AA^\top = \alpha I$. Contrary, we focus on the situation where we have many constraints with operators ($AA^\top \neq \alpha I$) that make generalized proximal mappings (12) difficult to compute. Below, we list additional benefits of our approach compared to existing packages that can solve intersection projection problems.

Contributions

Our aim is to design and implement parallel computational optimization algorithms for solving projection problems onto intersections of multiple constraint sets in the context of inverse problems. To arrive at this optimization framework, `SetIntersectionProjection`, we propose

- an implementation that avoids nesting of algorithms and exploits similarities between constraint sets, unlike black-box alternating projection methods such as Dykstra’s algorithm. Taking similarities between sets into account allows us to work with many sets at a relatively small increase in computational cost.

- algorithms that are based on a relaxed variant of the simultaneous direction method of multipliers [SDMM, Afonso et al., 2011, Combettes and Pesquet, 2011, Kitic et al., 2016]. By merging SDMM with recently developed schemes for automatically adapting the augmented-Lagrangian penalty and relaxation parameters [Xu et al., 2017b,a], we achieve speedups when solving problem (1) compared to the straightforward application of operator splitting methods.
- a software design specifically for set intersection projection problems. Our specializations enhance computational performance and include (i) a relatively simple multilevel strategy for ADMM-based algorithms that does part of the computations on coarser grids; (ii) solutions of banded linear systems in compressed diagonal format (CDS) with multi-threaded matrix-vector products (MVP). These MVPs are faster than general purpose storage formats like compressed sparse column storage (CSC) and support linear operators with spatially varying (blurring) kernels; (iii) more intuitive stopping criteria based on set feasibility.
- to make our work available as a software package in **Julia** [Bezanson et al., 2017]. Besides the algorithms, we also provide scripts for setting up the constraints, projectors and linear operators, as well as various examples. All presented timings, comparisons, and examples are reproducible.
- an implementation that is suitable for small matrices (2D) up to larger tensors (3D models, at least $m \in \mathbb{R}^{300 \times 300 \times 300}$). Because we solve simple-to-compute sub-problems in closed form and independently in parallel, the proposed algorithms work with large models and many constraints. We achieve this because there is only a single inexact linear-system solve that does not become much more computationally expensive as we add more constraint sets.

To demonstrate the capabilities of our optimization framework and implementation, we provide examples how projections onto an intersection of multiple constraint sets can be used to solve linear image processing tasks such as denoising an deconvolution and more complicated inverse problems including nonlinear parameters estimation problems with PDEs.

Notation, assumptions, and definitions

Our goal is to estimate the model vector (e.g., discretized medium parameters such as the acoustic wave speed) $m \in \mathbb{R}^N$, which in 2D corresponds to a vectorized (lexicographically ordered) matrix of size $n_z \times n_x$. Coordinate z is the vertical direction and x the horizontal direction. There are $N = n_x \times n_z$ elements in a 2D model. Our work applies to 2D and 3D models but to keep the derivations simpler we limit the descriptions to 2D models discretized on a regular grid. We use the following discretization for the vertical derivative in our constraint definitions

$$D_z = \frac{1}{h_z} \begin{pmatrix} -1 & 1 & & & \\ & -1 & 1 & & \\ & & \ddots & \ddots & \\ & & & -1 & 1 \end{pmatrix}, \quad (8)$$

where h_z is the vertical grid size. We define the discretized vertical derivative for the 2D model as the Kronecker product of D_z and the identity matrix corresponding to the x-dimension: $D_z \otimes I_x$.

The indicator function of a convex or non-convex set \mathcal{C} is defined as

$$\iota_{\mathcal{C}}(m) = \begin{cases} 0 & \text{if } m \in \mathcal{C}, \\ +\infty & \text{if } m \notin \mathcal{C}. \end{cases} \quad (9)$$

We define the Euclidean projection onto a set \mathcal{C} as

$$\mathcal{P}_{\mathcal{C}}(m) = \arg \min_x \|x - m\|_2^2 \quad \text{s.t.} \quad m \in \mathcal{C}. \quad (10)$$

This projection is unique if \mathcal{C} is a closed and convex set. If \mathcal{C} is a non-convex set, the projection may not be unique so the result is any vector in the set of minimizers of the projection problem. The proximal map of a function $g(m) : \mathbb{R}^N \rightarrow \mathbb{R} \cup \{+\infty\}$ is defined as

$$\text{prox}_{\gamma,g}(m) = \arg \min_x g(x) + \frac{\gamma}{2} \|x - m\|_2^2, \quad (11)$$

so $\text{prox}_{\gamma,g}(m) : \mathbb{R}^N \rightarrow \mathbb{R}^N$, where $\gamma > 0$ is a scalar. The case when $g(x)$ includes a linear operator $A \in \mathbb{R}^{M \times N}$ is of particular interest to us and we make it explicit with the definition

$$\text{prox}_{\gamma,g \circ A}(m) = \arg \min_x g(Ax) + \frac{\gamma}{2} \|x - m\|_2^2. \quad (12)$$

Even though $\text{prox}_{\gamma,g}(m)$ is often available in closed-form solution, or cheap to compute [Combettes and Pesquet, 2011, Parikh and Boyd, 2014, Beck, 2017, Chapter 6 & 7], $\text{prox}_{\gamma,g \circ A}(m)$ is usually not available in closed form if $AA^\top \neq \alpha I$, $\alpha > 0$ and more expensive to compute. Here, the symbol $^\top$ refers to (Hermitian) transpose. The proximal map for the indicator function is the projection:

$$\text{prox}_{\gamma,\iota_{\mathcal{C}}}(m) = \mathcal{P}_{\mathcal{C}}(m)$$

with $\mathcal{P}_{\mathcal{C}}(m)$ defined as in (10). The intersection of an arbitrary number of convex sets, $\bigcap_{i=1}^p \mathcal{C}_i$, is also convex. We assume that all constraints are chosen consistently, such that the intersection of all selected constraint sets is nonempty:

$$\bigcap_{i=1}^p \mathcal{C}_i \neq \emptyset. \quad (13)$$

This assumption is not restrictive in practice because apparently contradicting constraint sets often have a non-empty intersection. For example, ℓ_1 -norm based total-variation constraints and smoothness promoting constraints have at least one model in their intersection: a homogeneous model has a total-variation equal to 0 and maximal smoothness.

We use $m[i]$ to indicate entries of the vector m . Subscripts like y_i refer to one of the sub-vectors that are part of $\tilde{y} = (y_1^\top \ y_2^\top \ \dots \ y_p^\top)^\top$.

The Euclidean inner product of two vectors is denoted as $a^\top b$, and $\|a\|_2^2 = a^\top a$.

PARSDMM: Exploiting similarity between constraint sets

As we briefly mentioned in the introduction, we want to construct an algorithm to compute projections onto the intersection of multiple sets that (i) avoids nesting multiple algorithms if we do not know a projection onto one of the sets in closed-form; (ii) explicitly exploit similarities between the $i = 1, 2, \dots, p$ linear operators $A_i \in \mathbb{R}^{M_i \times N}$; (iii) do most computational work in parallel. The first step to accomplish this is writing each constraint set \mathcal{V}_i in problem (1) as the indicator function of a ‘simple’ set (\mathcal{C}_i) and a possibly non-orthogonal linear operator: $x \in \mathcal{V}_i \Leftrightarrow A_i x \in \mathcal{C}_i$. We formulate projection of $m \in \mathbb{R}^N$ onto the intersection of p sets as

$$\min_x \frac{1}{2} \|x - m\|_2^2 + \sum_{i=1}^p \iota_{\mathcal{C}_i}(A_i x). \quad (14)$$

In this section, we introduce our main algorithm, Projection Adaptive Relaxed Simultaneous Method of Multipliers (PARSDMM). The name derives from the relation to existing works about adaptive relaxation and ADMM-variants for minimizing sums of functions. It is designed to solve inverse problems that call for multiple pieces of prior knowledge in the form of constraints. Each piece of prior knowledge corresponds to

a single set. We focus on intersections up to about 16 sets, which we found adequate to regularize inverse problems. To avoid technical issues with non-convexity, we, for now, assume all sets to be closed and convex.

We use ADMM as a starting point. ADMM is known to solve intersection projection (and feasibility) problems [Boyd et al., 2011, Pakazad et al., 2015, Bauschke and Koch, 2015, Jia et al., 2017, Tibshirani, 2017, Kundu et al., 2017]. However, it remains a black-box algorithm and struggles with projections that do not have closed-form solutions. For completeness and to highlight the differences with the algorithm we propose below, we describe in Appendix A a black-box algorithm for the projection onto the intersection of sets based on ADMM.

The augmented Lagrangian

To start the derivation of PARSDMM, we introduce separate vectors $y_i \in \mathbb{R}^{M_i}$ for each of the $i = 1, \dots, p$ constraint sets of problem (14) and we add linear equality constraints as follows:

$$\min_{x, \{y_i\}} \frac{1}{2} \|x - m\|_2^2 + \sum_{i=1}^p \iota_{C_i}(y_i) \quad \text{s.t.} \quad A_i x = y_i. \quad (15)$$

The augmented Lagrangian [e.g., Nocedal and Wright, 2000, Chapter 17] of problem (15) is a basis for ADMM (see (19) below). To ensure that the x -minimization of the augmented Lagrangian remains quadratic, we make this minimization problem independent of the distance term $\frac{1}{2} \|x - m\|_2^2$. This choice has the additional benefit of allowing for other functions that measure distance from m . We remove the direct coupling of the distance term by (i) introducing the additional variables and constraints $y_{p+1} = A_{p+1}x = I_N x$; (ii) defining $\frac{1}{2} \|x - m\|_2^2 \equiv f(y_{p+1})$; (iii) creating the function

$$\tilde{f}(\tilde{y}) = f(y_{p+1}) + \sum_{i=1}^p \iota_{C_i}(y_i), \quad (16)$$

where we use the $\tilde{\cdot}$ symbol to indicate concatenated matrices and vectors, as well as functions that are the sum of multiple functions to simplify notation. The concatenated matrices and vectors read

$$\tilde{A} = \begin{pmatrix} A_1 \\ \vdots \\ A_{p+1} = I_N \end{pmatrix}, \quad \tilde{y} = \begin{pmatrix} y_1 \\ \vdots \\ y_{p+1} \end{pmatrix}, \quad \tilde{v} = \begin{pmatrix} v_1 \\ \vdots \\ v_{p+1} \end{pmatrix}. \quad (17)$$

The vectors $v_i \in \mathbb{R}^{M_i}$ are the Lagrangian multipliers that occur in the augmented Lagrangian for the projection problem. We always have $A_{p+1}x = I_N x = y_{p+1}$ for the Euclidean projection that uses the squared ℓ_2 -distance $\frac{1}{2} \|x - m\|_2^2$. With these new definitions, problem (15) becomes

$$\min_{x, \tilde{y}} \tilde{f}(\tilde{y}) \quad \text{s.t.} \quad \tilde{A}x = \tilde{y}. \quad (18)$$

This formulation has the same form as problems that regular ADMM solves—i.e., $\min_{x,y} f(x) + g(y)$ s.t. $Ax + By = c$. It follows that we can guarantee convergence under the same conditions as for ADMM. According to [Boyd et al., 2011, Eckstein and Yao, 2015], ADMM converges when $f(x) : \mathbb{R}^{N_1} \rightarrow \mathbb{R} \cup \{+\infty\}$ and $g(y) : \mathbb{R}^{N_2} \rightarrow \mathbb{R} \cup \{+\infty\}$ are proper and convex. The linear equality constraints involve matrices $A \in \mathbb{R}^{M \times N_1}$ and $B \in \mathbb{R}^{M \times N_2}$ and vectors $x \in \mathbb{R}^{N_1}$, $y \in \mathbb{R}^{N_2}$ and $c \in \mathbb{R}^M$.

To arrive at the main iterations of PARSDMM, we continue based on the augmented Lagrangian for (18), which reads

$$L_{\rho_1, \dots, \rho_{p+1}}(x, y_1, \dots, y_{p+1}, v_1, \dots, v_{p+1}) = \sum_{i=1}^{p+1} \left[f_i(y_i) + v_i^\top (y_i - A_i x) + \frac{\rho_i}{2} \|y_i - A_i x\|_2^2 \right]. \quad (19)$$

As we can see, this expression has a separable structure with respect to the Lagrangian multipliers v_i , and the auxiliary vectors y_i . Following the ADMM variants for multiple functions, as formulated by [Song et al., 2016, Kitic et al., 2016, Xu et al., 2017c], we use a different penalty parameter $\rho_i > 0$ for each index i . In this way, we make sure all linear equality constraints $A_i x = y_i$ are satisfied sufficiently when running a limited number of iterations. Because the different matrices A_i may have widely varying scalings and sizes, a fixed penalty for all i could cause slow convergence of x towards one of the constraint sets. To further accelerate the algorithm we also introduce a different relaxation parameter (γ_i) for each index i . After we derive the main steps of our proposed algorithm, we describe the automatic selection of the scalar parameters.

The iterations

With the above definitions, iteration counter k , and inclusion of relaxation parameters, which we assume to be limited to the interval $\gamma_i \in [1, 2)$ [see Xu et al., 2017b], the iterations can be written as

$$\begin{aligned}
x^{k+1} &= \arg \min_x \sum_{i=1}^{p+1} \left(\frac{\rho_i^k}{2} \|y_i^k - A_i x + \frac{v_i^k}{\rho_i^k}\|_2^2 \right) \\
\bar{x}_i^{k+1} &= \gamma_i^k A_i x_i^{k+1} + (1 - \gamma_i^k) y_i^k \\
y_i^{k+1} &= \arg \min_{y_i} \left[f_i(y_i) + \frac{\rho_i^k}{2} \|y_i^k - \bar{x}_i^{k+1} + \frac{v_i^k}{\rho_i^k}\|_2^2 \right] \\
v_i^{k+1} &= v_i^k + \rho_i^k (y_i^{k+1} - \bar{x}_i^{k+1}).
\end{aligned} \tag{20}$$

To arrive at our final algorithm, we rewrite these iterations in a more explicit form as

$$\begin{aligned}
x^{k+1} &= \left[\sum_{i=1}^p (\rho_i^k A_i^\top A_i) + \rho_{p+1}^k I_N \right]^{-1} \sum_{i=1}^{p+1} \left[A_i^\top (\rho_i^k y_i^k + v_i^k) \right] \\
\bar{x}_i^{k+1} &= \gamma_i^k A_i x_i^{k+1} + (1 - \gamma_i^k) y_i^k \\
y_i^{k+1} &= \text{prox}_{f_i, \rho_i^k} \left(\bar{x}_i^{k+1} - \frac{v_i^k}{\rho_i^k} \right) \\
v_i^{k+1} &= v_i^k + \rho_i^k (y_i^{k+1} - \bar{x}_i^{k+1}).
\end{aligned} \tag{21}$$

In this expression, we used the fact that A_{p+1} is always the identity matrix of size N for projection problems. Without over/under relaxation [\bar{x}_i^{k+1} computation, Eckstein and Bertsekas, 1992, Iutzeler and Hendrickx, 2017, Xu et al., 2017b], these iterations are known as SALSA [Afonso et al., 2011] or the simultaneous direction method of multipliers [SDMM, Combettes and Pesquet, 2011, Kitic et al., 2016]. The derivation in this section shows that ADMM/SDMM solve the projection onto an intersection of multiple closed and convex sets. However, the basic iterations from (21) are not yet a practical and fast algorithm, because there are scalar parameters that need to be selected, no stopping conditions, and no specializations to constraints typically found in the imaging sciences. We address these issues in the following sections.

Computing the proximal maps

The proximal maps in the iterations (21) become projections onto simple sets (e.g., bounds/ ℓ_1 and ℓ_2 norm-ball/cardinality/rank), which permit closed-form solutions that do not depend on the ρ_i . When $f_{p+1}(w) = 1/2 \|w - m\|_2^2$, (squared ℓ_2 distance of w to the reference vector m) the proximal map is also available in closed form:

$$\begin{aligned}
\text{prox}_{f_{p+1}, \rho_{p+1}}(w) &= \arg \min_z 1/2 \|z - m\|_2^2 + \rho_{p+1}/2 \|z - w\|_2^2 \\
&= (m + \rho_{p+1} w) / (1 + \rho_{p+1}),
\end{aligned} \tag{22}$$

where we understand the division in a point-wise sense. We thus avoided other convex optimization algorithms for computations of the proximal maps of interest.

Solving the linear system and automatic parameter selection

We can see from (21) that the computation of x^{k+1} involves the solution of a single system of normal equations that contains all linear operators. The system matrix equals

$$C \equiv \sum_{i=1}^{p+1} (\rho_i A_i^\top A_i) = \sum_{i=1}^p (\rho_i A_i^\top A_i) + \rho_{p+1} I_N \quad (23)$$

and is by construction always positive-definite because $\rho_i > 0$ for all i . The minimization over x is therefore uniquely defined. As suggested by Xu et al. [2017a], we adapt the ρ_i 's every two iterations using the scheme we discuss below.

While we could use direct matrix factorizations of C , we would need to refactorize every time we update any of the ρ_i 's. This makes computing x^{k+1} too costly. Instead, we rely on warm-started iterative solvers with x^k used as the initial guess for x^{k+1} . There exist several alternatives including LSQR [Paige and Saunders, 1982] to solve the above linear system (x^{k+1} computation in 21) iteratively. We choose to apply the conjugate-gradient (CG) method to the normal equations for the following reasons:

1. Contrary to LSQR, transforms that satisfy $A_i^\top A_i = \alpha I_N$ are free in CG because we explicitly form the sparse system matrix C , which already includes the identity matrix.
2. By limiting the relative difference between the ρ_i and ρ_{p+1} , where the latter corresponds to the identity matrix in (23), we ensure C is sufficiently well conditioned so squaring the condition number does not become a numerical problem.
3. For many transforms, the matrices $A_i^\top A_i$ are sparse and have at least partially overlapping sparsity patterns (discrete derivative matrices for one or more directions, orthogonal transforms). Multiplication with $\sum_{i=1}^{p+1} (\rho_i A_i^\top A_i)$ is therefore not much more expensive than multiplication with a single $A_i^\top A_i$. However, LSQR requires matrix-vector products with all A_i and A_i^\top at every iteration.
4. Full reassembly of C at iteration k is not required. Every time we update any of the ρ_i , we update C by subtracting and adding the block corresponding to the updated ρ_i . If the index that changed is indicated by $i = u$, the system matrix for the next x^{k+1} computation becomes

$$\begin{aligned} C^{k+1} &= \sum_{i=1}^{p+1} (\rho_i^{k+1} A_i^\top A_i) = \sum_{i=1}^{p+1} (\rho_i^k A_i^\top A_i) - (\rho_u^k A_u^\top A_u) + (\rho_u^{k+1} A_u^\top A_u) \\ &= C^k + A_u^\top A_u (\rho_u^{k+1} - \rho_u^k). \end{aligned} \quad (24)$$

For each ρ_i update, forming the new system matrix involves a single addition of two sparse matrices (assuming all $A_i^\top A_i$'s are pre-computed).

To further save computation time, we solve the minimization with respect to x inexactly. We select the stopping criterion for CG adaptively in terms of the relative residual of the normal equations—i.e., we stop CG if the relative residual drops below

$$0.1 \left\| \left[\sum_{i=1}^{p+1} (\rho_i^k A_i^\top A_i) \right] x - \sum_{i=1}^{p+1} \left[A_i^\top (\rho_i^k y_i^k + v_i^k) \right] \right\|_2 / \left\| \sum_{i=1}^{p+1} \left[A_i^\top (\rho_i^k y_i^k + v_i^k) \right] \right\|_2. \quad (25)$$

Empirically, we found this choice robust and it also results in time savings for solving problem (18) compared to a fixed and accurate stopping criterion for the x -minimization step. The stopping criterion for CG is relatively inexact during the first few iterations from (21) and requests more accurate solutions later on, such that the conditions on inexact sub-problem solutions from [Eckstein and Bertsekas, 1992] will be satisfied eventually.

Just like standard ADMM, our algorithm may also need a large number of iterations (21) for a fixed penalty parameter ρ_i for all i [e.g., Nishihara et al., 2015, Xu et al., 2017a]. It is better to update ρ_i^k and γ_i^k every couple of iterations to ensure we reach a good solution in a relatively small number of iterations. For this purpose, we use Xu et al. [2017a]’s automatic selection of ρ_i^k and γ_i^k for ADMM. Numerical experiments by Xu et al. [2016] show that these updates also perform well on various non-convex problems. The updates themselves are based on a Barzilai-Borwein spectral step size [Barzilai and Borwein, 1988] for Douglas-Rachford (DR) splitting applied to the dual of $\min_{x,y} f(x) + g(y)$ s.t. $Ax + By = c$ and derive from equivalence between ADMM and DR [Eckstein and Bertsekas, 1992, Esser, 2009].

Exploiting parallelism

Given the grid size of 3D PDE-based parameter estimation problems and our desire to work with multiple constraint sets, we seek a parallel implementation that exploits multi-threading offered by programming languages such as Julia [Bezanson et al., 2017]. Since the computational time for the x -minimization using the conjugate-gradient algorithm is dominated by the matrix-vector products (MVP) with C , we concentrate our efforts there by using compressed diagonal storage (CDS), see, e.g., Saad [1989]; Serón et al. [1990]; Kotakemori et al. [2008]. This format stores the non-zero bands of the matrix as a dense matrix, and we compute MVPs directly in this storage system. These MVPs are faster than the more general Compressed Sparse Column (CSC) format. CDS has the additional benefit that it can efficiently handle matrices generated by spatially varying (blurring, derivative) kernels. We can use CDS if all matrices $A_i^T A_i$ have a banded sparsity-pattern. Using Julia’s multi-threading, we compute the MVPs with C in parallel. In cases where the $A_i^T A_i$ ’s do not have a banded structure we revert to computations in the standard CSC format.

Aside from matrix-vector products during the inner iterations, most calculation time in (21) is used for \bar{x}_i^{k+1} , y_i^{k+1} , v_i^{k+1} , ρ_i^{k+1} , and γ_i^{k+1} . To reduce these computation times, we compute these quantities in parallel. This is relatively straightforward to do because each problem is independent so that the operations for the p constraints can be carried out by different Julia workers where each worker either uses Julia threads, multi-threaded BLAS [OpenBLAS, Wang et al., 2013], or multi-threaded Fourier-transforms [FFTW library, Frigo and Johnson, 2005].

Stopping conditions

So far, we focussed on reducing the time for each iteration of (21). However, fast solutions to the full problem are possible only if we know when to stop iterating. When working with a single constraint set, stopping criteria based on a combination of the primal $r^{\text{pri}} = \|\tilde{y} - \tilde{A}x^k\|$ and dual residual $r^{\text{dual}} = \|\tilde{\rho}\tilde{A}^T(\tilde{y}^k - \tilde{y}^{k-1})\|$ are adequate as long as both become sufficiently small [e.g., Boyd et al., 2011, Kitic et al., 2016, Xu et al., 2017a]. However, the situation is more complicated in situations where we work with multiple constraint sets. In that case, the \tilde{y} and \tilde{A} contain a variety of vectors and linear operators that correspond to the different constraint sets. It then becomes more difficult to determine the relationship between the size of the residuals and the distance to each set. With other words, it becomes challenging to decide at what primal and dual residual to stop such that we are close to all constraint sets.

Instead, it may be more intuitive to look at the feasibility for each set separately. This holds if x is in the intersection of the constraint sets but requires computationally costly projections onto each \mathcal{V}_i to verify, a

situation we want to avoid in PARSDMM. Instead, we rely on the transform-domain set feasibility error

$$r_i^{\text{feas}} = \frac{\|A_i x - \mathcal{P}_{\mathcal{C}_i}(A_i x)\|}{\|A_i x\|}, i = 1 \cdots p, \quad (26)$$

to which we have access at a relatively low cost since we already computed $A_i x$ in the iterations from (21). Our first stopping criterion thus corresponds to a normalized version of the objective Censor et al. [2005] uses when solving convex multiple set split-feasibility problems. We added this normalization in (26) to account for different types and sizes of the linear operators A_i . The projections onto the constraint sets $\mathcal{P}_{\mathcal{C}_i}(\cdot)$ themselves, are relatively cheap to compute since they only include projections onto ‘simple’ sets based on norm-balls, bounds, cardinality, and matrix rank. By testing for transform-domain feasibility every few iterations only (typically 5), we further reduce the computational costs for our stopping condition.

Satisfying constraints does not indicate whether or not x^k is close to the projection onto the intersection of the p different constraint sets or if it is just a feasible point, possibly ‘deep’ inside the intersection. If x^k is indeed the projection of m , then $\|x^k - x^{k-1}\|$ approaches a stationary point, assuming that x^k converges to the projection. We make this property explicit by considering the maximum relative change of x^k over the s previous iterations: $j \in S \equiv \{1, 2, \dots, s\}$. The relative evolution of x at the k th iteration thus becomes

$$r^{\text{evol}} = \frac{\max_{j \in S} \{\|x^k - x^{k-j}\|\}}{\|x^k\|}. \quad (27)$$

By considering the history (we use $s = 5$ in our numerical examples), our stopping criterion becomes more robust to oscillations in $\|x^k - x^{k-1}\|$ as a function of k . So we propose to stop PARSDMM if

$$r^{\text{evol}} < \varepsilon^{\text{evol}} \quad \text{and} \quad r_i^{\text{feas}} < \varepsilon_i^{\text{feas}} \quad \forall i. \quad (28)$$

During our numerical experiments, we select $\varepsilon^{\text{evol}} = 10^{-2}$ and $\varepsilon_i^{\text{feas}} = 10^{-3}$, which balance sufficiently accurate solutions and short solution times. These are still two constants to be chosen by the user, but we argue that r_i^{feas} may relate better to our intuition on feasibility because it behaves like a distance to each set separately. The evolution term $\|x^k - x^{k-1}\|$ is found in many optimization algorithms and is especially informative for physical parameter estimation problems where practitioners often have a good intuition to which $\|x^k - x^{k-1}\|$ the physical forward operator is sensitive.

The PARSDMM algorithm

We summarize our discussions from the previous sections in the following Algorithms.

Multilevel PARSDMM

Inverse problems with PDE forward models typically need a fine grid for stable physical simulations. At the same time, we often use constraints to estimate ‘simple’ models—i.e. models that are smooth, have a low-rank, are sparse in some transform-domain, and that may not need many grid points for accurate representations of the image/model. This suggests we can reduce the total computational time of PARSDMM (Algorithm 1) by using a multilevel continuation strategy [see, e.g., Nash, 2000, Ascher and Haber, 2001, Nash, 2014, Parpas, 2017]. The multilevel idea presented in this section applies to the projection onto the intersection of constraint sets only and not to the grids for solving PDEs. Our approach proceeds as follows: we start at a coarse grid and continue towards finer grids without cycling between coarse and fine grids. By using the solution at the coarse grid as the initial guess for the solution on the finer grid, the convergence guarantees are the same as for the single level version of our algorithm. This multilevel approach is similar to multilevel ADMM by Macdonald and Ruthotto [2018] for non-convex linear equality constrained problems. Numerical experiments in the following section show reduced solution times and better performance on non-convex problems.

Algorithm 1 Projection Adaptive Relaxed Simultaneous Direction Method of Multipliers (PARSDMM) to compute the projection onto an intersection, including automatic selection of the penalty parameters and relaxation.

Algorithm PARSDMM

inputs:

m //point to project
 $A_1, A_2, \dots, A_p, A_{p+1} = I_N$ //linear operators
 $\text{prox}_{f_i, \rho_i}(w) = \mathcal{P}_{C_i}(w)$ for $i = 1, 2, \dots, p$ //norm/bound/cardinality/... projectors
 $\text{prox}_{f_i, \rho_{p+1}}(w) = (m + \rho_{p+1}w)/(1 + \rho_i)$ //prox for the squared distance from m
select ρ_i^0, γ_i^0 , update-frequency for γ and ρ
optional: initial guess for x, y_i and v_i

initialize:

$B_i = A_i^\top A_i$ //pre-compute for all i
 $C = \sum_{i=1}^{p+1} (\rho_i B_i)$ //pre-compute
 $k = 1$

WHILE not converged

$x^{k+1} = C^{-1} \sum_{i=1}^{p+1} [A_i^\top (\rho_i^k y_i^k + v_i^k)]$ //CG, stop when (25) holds

FOR $i = 1, 2, \dots, p + 1$ //compute in parallel

$s_i^{k+1} = A_i x^{k+1}$

$\bar{x}_i^{k+1} = \gamma_i^k s_i^{k+1} + (1 - \gamma_i^k) y_i^k$

$y_i^{k+1} = \text{prox}_{f_i, \rho_i}(\bar{x}_i^{k+1} - \frac{v_i^k}{\rho_i^k})$

$v_i^{k+1} = v_i^k + \rho_i^k (y_i^{k+1} - \bar{x}_i^{k+1})$

stop if conditions (28) hold

If $\text{mod}(k, \text{update-frequency}) = 1$

$\{\rho_i^{k+1}, \gamma_i^{k+1}\} = \text{adapt-rho-gamma}(v_i^k, v_i^{k+1}, y_i^{k+1}, s_i^{k+1}, \rho_i^k)$

End if

END

FOR $i = 1, 2, \dots, p + 1$ //update C if necessary

If $\rho_i^{k+1} \neq \rho_i^k$

$C \leftarrow C + B_i(\rho_i^{k+1} - \rho_i^k)$

End if

END

$k \leftarrow k + 1$

END

output: x

Different from many applications of multilevel algorithms, is that we are not interested in approximating the primal variable x , because ADMM-type iterations compute this quantity in the first step, see Algorithm 1. Instead, we need to concern ourselves with the initial guesses of auxilliary variables y_i and Lagrangian multipliers v_i for all $i \in \{1, \dots, p, p + 1\}$. After initialization of the coarsest grid with all zero vectors, we move to a finer grid by interpolating y_i and v_i . Since the solution estimate $x \in \mathbb{R}^N$ always refers to an image (2D/3D) for our applications, we know that v_i and y_i relate to images as well and their dimensions depend on the corresponding A_i . Therefore we interpolate y_i and v_i as images.

Example. When A_i is a discrete derivative matrix, then the vectors v_i and y_i live on a grid that we know at every level of the multilevel scheme. If we have $A_i = D_z \otimes I_x$, where D_z is the first-order finite-difference matrix as in (8), we know that $A_i \in \mathbb{R}^{(n_z-1)n_x \times (n_z \times n_x)}$ and therefore $v_i \in \mathbb{R}^{(n_z-1)n_x}$ and $y_i \in \mathbb{R}^{(n_z-1)n_x}$. We can thus reshape the associated vectors v_i and y_i as an image (in 2D) of size $(n_z - 1 \times n_x)$ and interpolate it to the finer grid for the next level, working from coarse to fine. In 3D, we follow the same approach. We

Algorithm 2 Adapt ρ and γ according to [Xu et al., 2017b] with some modifications to save computational work. The constant $\varepsilon^{\text{corr}}$ is in the range $[0.1 - 0.4]$ as suggested by [Xu et al., 2017b]. Quantities from the previous call to adapt-rho-gamma have the indication k_0 . Actual implementation computes and re-uses some of the inner products and norms.

Algorithm **adapt-rho-gamma**

input: $v_i^k, v_i^{k+1}, y_i^{k+1}, s_i^{k+1}, \rho_i^k$

$\varepsilon^{\text{corr}} = 0.3$

$$\hat{v}^{k+1} = v_i^k + \rho_i^k (y_i^k - s_i^{k+1})$$

$$\Delta \hat{v} = \hat{v}_i^{k+1} - \hat{v}_i^{k_0}$$

$$\Delta v = v_i^{k+1} - v_i^{k_0}$$

$$\Delta \hat{h} = s_i^{k+1} - s_i^{k_0}$$

$$\Delta \hat{g} = -(y_i^{k+1} - y_i^{k_0})$$

$$\alpha^{\text{corr}} = \frac{\Delta \hat{h}^\top \Delta \hat{v}}{\|\Delta \hat{h}\| \|\Delta \hat{v}\|}$$

$$\beta^{\text{corr}} = \frac{\Delta \hat{g}^\top \Delta v}{\|\Delta \hat{g}\| \|\Delta v\|}$$

If $\alpha^{\text{corr}} > \varepsilon^{\text{corr}}$

$$\hat{\alpha}^{\text{MG}} = \frac{\Delta \hat{h}^\top \Delta \hat{v}}{\Delta \hat{h}^\top \Delta \hat{h}}, \hat{\alpha}^{\text{SD}} = \frac{\Delta \hat{v}^\top \Delta \hat{v}}{\Delta \hat{h}^\top \Delta \hat{v}}, \hat{\alpha} = \begin{cases} \hat{\alpha}^{\text{MG}} & \text{if } 2\hat{\alpha}^{\text{MG}} > \hat{\alpha}^{\text{SD}} \\ \hat{\alpha}^{\text{SD}} - 0.5\hat{\alpha}^{\text{MG}} & \text{if else} \end{cases}$$

End

If $\beta^{\text{corr}} > \varepsilon^{\text{corr}}$

$$\hat{\beta}^{\text{MG}} = \frac{\Delta \hat{g}^\top \Delta v}{\Delta \hat{g}^\top \Delta \hat{g}}, \hat{\beta}^{\text{SD}} = \frac{\Delta v^\top \Delta v}{\Delta \hat{g}^\top \Delta v}, \hat{\beta} = \begin{cases} \hat{\beta}^{\text{MG}} & \text{if } 2\hat{\beta}^{\text{MG}} > \hat{\beta}^{\text{SD}} \\ \hat{\beta}^{\text{SD}} - 0.5\hat{\beta}^{\text{MG}} & \text{if else} \end{cases}$$

End

$$\{\rho^{k+1}, \gamma^{k+1}\} = \begin{cases} \left\{ \sqrt{\hat{\alpha}\hat{\beta}}, 1 + \frac{2\sqrt{\hat{\alpha}\hat{\beta}}}{\hat{\alpha} + \hat{\beta}} \right\} & \text{if } \alpha^{\text{corr}} > \varepsilon^{\text{corr}} \ \& \ \beta^{\text{corr}} > \varepsilon^{\text{corr}} \\ \{\hat{\alpha}, 1.9\} & \text{if } \alpha^{\text{corr}} > \varepsilon^{\text{corr}} \ \& \ \beta^{\text{corr}} \leq \varepsilon^{\text{corr}} \\ \{\hat{\beta}, 1.1\} & \text{if } \alpha^{\text{corr}} \leq \varepsilon^{\text{corr}} \ \& \ \beta^{\text{corr}} > \varepsilon^{\text{corr}} \\ \{\rho^k, 1.5\} & \text{if } \alpha^{\text{corr}} \leq \varepsilon^{\text{corr}} \ \& \ \beta^{\text{corr}} \leq \varepsilon^{\text{corr}} \end{cases}$$

set $\hat{v}^{k_0} \leftarrow \hat{v}_i^{k+1}$, $v^{k_0} \leftarrow v_i^{k+1}$, $s^{k_0} \leftarrow s_i^{k+1}$, $y^{k_0} \leftarrow y_i^{k+1}$ and save for next call to **adapt-rho-gamma**

save v_i^{k+1}, y_i^{k+1} for next call to **adapt-rho-gamma**

output: $\rho_i^{k+1}, \gamma_i^{k+1}$

also need a coarse version of m at each level: m_l for $l = n_{\text{levels}}, n_{\text{levels}} - 1, \dots, 1$. We simply obtain the coarse models by applying anti-alias filtering and subsampling of the original m . In principle, any subsampling and interpolation technique may be used in this multilevel framework, because it just constructs initial guesses for the next levels.

We decide the number of levels (n_{levels}) and the coarsening factor ahead of time. Together with the original grid, these determine the grid at all levels so we can set up the linear operators and proximal mappings at each level. This set-up phase is a one time cost since its result is reused every time we project a model m onto the intersection of constraint sets. The additional computational costs of the multilevel scheme are the interpolation of all y_i and v_i to a finer grid, but this happens only once per level and not every ML-PARSDMM (Algorithm 3) iteration. So the computational overhead we incur from the interpolations is small compared to the speedups that Algorithm 3 offers.

Algorithm 3 Multilevel PARSDMM to compute the projection onto an intersection of sets.

inputs:

```

 $n_{\text{levels}}$  //number of levels
 $l = \{n_{\text{levels}}, n_{\text{levels}} - 1, \dots, 1\}$ 
 $\text{grid}_l$  //grid info at each level  $l$ 
 $m_l$  //model to project at every level  $l$ 
 $A_{1,l}, A_{2,l}, \dots, A_{p+1,l}$  //linear operators at every level
// norm/bound/cardinality/... projectors at each level:
 $\text{prox}_{f_{i,l}, \rho_i}(w) = \mathcal{P}_{C_{i,l}}(w)$  for  $i = 1, 2, \dots, p$ 
// proximal map for the squared distance from  $m$  at each level:
 $\text{prox}_{f_{p+1,l}, \rho_{p+1}}(w) = (m_l + \rho_{p+1}w)/(1 + \rho_{p+1})$ 
//start at coarsest grid
FOR  $l = n_{\text{levels}}, n_{\text{levels}} - 1, \dots, 1$ 
  //solve on current grid
   $(x_l, \{y_{i,l}\}, \{v_{i,l}\}) = \text{PARSDMM}(m_l, \{A_{i,l}\}, \{\text{prox}_{f_{i,l}, \rho_i}\}, x_l, \{y_{i,l}\}, \{v_{i,l}\})$ 
   $x_l \rightarrow x_{l-1}$  //interpolate to finer grid
  FOR  $i = 1, 2, \dots, p + 1$ 
     $y_{i,l} \rightarrow y_{i,l-1}$  //interpolate to finer grid
     $v_{i,l} \rightarrow v_{i,l-1}$  //interpolate to finer grid
  END
END
output:  $x$  at original grid (level 1)

```

Software and numerical examples

The software corresponding to this paper is available at <https://github.com/slimgroup/SetIntersectionProjection.jl>. All algorithms, examples, and utilities to set up the projectors and linear operators are included. Our software is specialized to the specific and fixed problem structure (14) with the flexibility to work with multiple linear operators and projectors. Because of these design choices, the user only needs to provide the model to project, m , and pairs of linear operators and projectors onto simple sets: $\{(A_1, \mathcal{P}_{C_1}), (A_2, \mathcal{P}_{C_2}), \dots, (A_p, \mathcal{P}_{C_p})\}$. The software adds the identity matrix and the proximal map for the distance squared from m . These are all computational components required to solve intersection projection problems as formulated in (16). No internal reformulation is required by our software.

To reap benefits from modern programming language design, including just-in-time compilation, multiple dispatch, and mixing distributed and multi-threaded computations, we wrote our software package in Julia. Our code uses parametric typing, which means that the same scripts can run in `Float32` (single) and `Float64` (double) precision. As expected, most components of our software run faster in `Float32` with reduced memory consumption. The timings in the following examples use `Float32`.

We provide scripts that set up the linear operators and projectors for regular grids in 2D and 3D. It is not necessary to use these scripts as the solver is agnostic to the specific construction of the projectors or linear operators. Table (1) displays the constraints we currently support. For example, when the user requests the script to set up minimum and maximum bounds on the discrete gradient in the z -direction of the model, the script returns the discrete derivative matrix $A = D_z \otimes I_x$ and a function $\mathcal{P}_{\text{bounds}}(\cdot)$ that projects the input onto the bounds. The software currently supports the identity matrix, matrices representing the discrete gradient and the operators that we apply matrix-free: the discrete cosine/Fourier/wavelet/curvelet [Ying et al., 2005] transforms.

For the special case of orthogonal linear operators, we leave the linear operator inside the set definition because we know the projection onto \mathcal{V} in closed form. For example, if $\mathcal{V} = \{x \mid \|Ax\|_1 \leq \sigma\}$ with discrete Fourier

descriptions	set
bounds	$\{m \mid l[i] \leq (Am)[i] \leq b[i]\}$
ℓ_1	$\{m \mid \ Am\ _1 \leq \sigma\}$
ℓ_2	$\{m \mid \ Am\ _2 \leq \sigma\}$
annulus	$\{m \mid \sigma_l \leq \ Am\ _2 \leq \sigma_u\}$
nuclear norm	$\{m \mid \sum_{j=1}^k \lambda[j] \leq \sigma\}$, with $Am = \text{vec}(\sum_{j=1}^k \lambda[j] u_j v_j^\top)$ is the SVD.
cardinality	$\{m \mid \text{card}(Am) \leq k\}$, k is a positive integer
rank	$\{m \mid \text{card}(\lambda) \leq r\}$, with $Am = \text{vec}(\sum_{j=1}^k \lambda[j] u_j v_j^\top)$ is the SVD and $r < \min(n_z, n_x)$
subspace constraints	$\{m \mid m = Ac, c \in \mathbb{R}^M\}$

Table 1: Overview of constraint sets that the software currently supports. A new constraint requires the projector onto the set (without linear operator) and a linear operator or equivalent matrix-vector product together with its adjoint. Vector entries are indexed as $m[i]$, u_j and v_j^\top indicate singular vectors.

transform (DFT) matrix $A \in \mathbb{C}^{N \times N}$, the projection is known in closed form as $\mathcal{P}_V(x) = A^* \mathcal{P}_{\|\cdot\| \leq \sigma}(Ax)$, where $*$ denotes the complex-conjugate transpose and $\mathcal{P}_{\|\cdot\| \leq \sigma}$ is the projection onto the ℓ_1 -ball. We do this to keep all other computations in PARSDMM (Algorithm 1) real, because complex-valued vectors require more storage and will slow down most computations.

Our software also allows to simultaneously use constraints that apply to the 2D/3D model and constraints that apply to each column/row/fiber separately. The linear operator remains the same if we define constraints for all rows, columns, or both. The difference is that the projection onto a simple set is now applied to each row/column independently in parallel via a multi-threaded loop.

As an example of our code, we show how to project a 2D model, m , onto the intersection of bound constraints and the set of models that have monotonically increasing parameter values in the z-direction.

using SetIntersectionProjection

```
#set up structure with grid information
mutable struct compgrid
    d :: Tuple
    n :: Tuple
end

#load a model
#m =

#the following optional lines of
#code set up linear operators and projectors

#grid information ( (dz,dx),(nz,nx) )
comp_grid = compgrid( (25.0, 6.0), (size(m,1), size(m,2)) )
m = vec(m) #algorithms take vectorized input

#initialize constraint information
constraint = Vector{SetIntersectionProjection.set_definitions}()

#set up bound constraints
min          = 1500.0          #minimum velocity
```

```

max           = 4500.0           #maximum velocity
set_type      = "bounds"        #bound constraint set
TD_OP        = "identity"       #identity matrix in the set definition
app_mode      = ("matrix", "")  #bounds applied to the model as a matrix
custom_OP     = ([], false)     #no custom linear operators

push!(constraint, set_definitions(set_type, TD_OP, min, max, app_mode, custom_OP))

#bounds on parameters in a transform-domain (vertical slope constraint)
min           = 0.0
max           = 1e6
set_type      = "bounds"
TD_OP        = "D_z"           #discrete derivative in z-direction
app_mode      = ("matrix", "")
custom_TD_OP  = ([], false)

push!(constraint, set_definitions(set_type, TD_OP, min, max, app_mode, custom_OP))

options = PARSDMM_options() #get default options
options.FL = typeof(m[1,1]) # get precision

#get projectors onto simple sets, linear operators, set information
(P_sub, TD_OP, set_Prop) = setup_constraints(constraint, comp_grid, options.FL)

#precompute and distribute quantities once, reuse later
(TD_OP, B, ~, ~) = PARSDMM_precompute_distribute(TD_OP, set_Prop, comp_grid, options)

#project onto intersection
(x, log_PARSDMM) = PARSDMM(m, B, TD_OP, set_Prop, P_sub, comp_grid, options)

```

Parallel Dykstra versus PARSDMM

To see if our new algorithm is faster than black-box type projection algorithms, such as parallel Dykstra’s algorithm (see Appendix A), we use Adaptive Relaxed ADMM (ARADMM) [Xu et al., 2017b] for the projection sub-problems of parallel Dykstra’s algorithm. Both PARSDMM (Algorithm 1) and Parallel Dykstra-ARADMM have the same computational components. ARADMM also uses the same update scheme for the augmented Lagrangian penalty and relaxation parameters as we use in PARSDMM. This similarity allows for a comparison of the convergence as a function of the basic computational components. We manually tuned ARADMM stopping conditions to achieve the best performance for parallel Dykstra’s algorithm overall.

The first numerical experiment is the projection of a 2D geological model (341×400 pixels) onto the intersection of three constraint sets that are of interest to seismic imaging [Esser et al., 2018, Peters et al., 2018, Yong et al., 2018]:

1. $\{m \mid \sigma_1 \leq m[i] \leq \sigma_2\}$: bound constraints
2. $\{m \mid \|Am\|_1 \leq \sigma\}$ with $A = \begin{pmatrix} D_z \otimes I_x \\ I_z \otimes D_x \end{pmatrix}$: anisotropic total-variation constraints
3. $\{m \mid 0 \leq ((D_z \otimes I_x)m)[i] \leq \infty\}$: vertical monotonicity constraints

For these sets, the primary computational components are

- matrix-vector products in the conjugate-gradient algorithm. Parallel Dykstra’s algorithms uses matrix-vector products with $A^\top A$, $(D_z \otimes I_x)^\top (D_z \otimes I_x)$, and I in parallel. PARSDMM computes matrix-vector products with the sparsity pattern of $A^\top A$ (this pattern overlaps with the the linear operators in the other two sets).
- projections onto the box constraint set and the ℓ_1 -ball. Both parallel Dykstra’s algorithm and PARSDMM compute these in parallel.
- parallel communication that sends a vector from one to all parallel processes (x^{k+1} in Algorithm 1), and one map-reduce parallel sum that gathers the sum of vectors on all workers (the right-hand side for the x^{k+1} computation in Algorithm 1). The communication is the same for PARSDMM and parallel Dykstra’s algorithm so we ignore it in the experiments below.

Before we show the numerical results, we discuss how we count the computational operations mentioned above.

- Matrix-vector products in CG: Parallel Dykstra’s algorithm simultaneously computes three projections by running three instances of ARADMM in parallel. For each parallel Dykstra iteration, we add the maximum number of CG iterations, corresponding to one of the sub-problems.
- ℓ_1 -ball projections: PARSDMM projects onto the ℓ_1 ball once per iteration. Parallel Dykstra projects (number of parallel Dykstra iterations) \times (number of ARADMM iterations for set number two) times onto the ℓ_1 ball. We focus on the ℓ_1 -ball projections [Duchi et al., 2008], because these projections are computationally more intensive compared to projections onto the box (element-wise comparison) and also less suitable for multi-threaded parallelization.

The results in Figure 1 show that PARSDMM requires much fewer CG iterations and ℓ_1 -ball projections to achieve the same relative set feasibility error in the transform-domain as defined in equation (26). We observe a somewhat oscillatory convergence of PARSDMM, which is caused by changing the relaxation and augmented-Lagrangian penalty parameters.

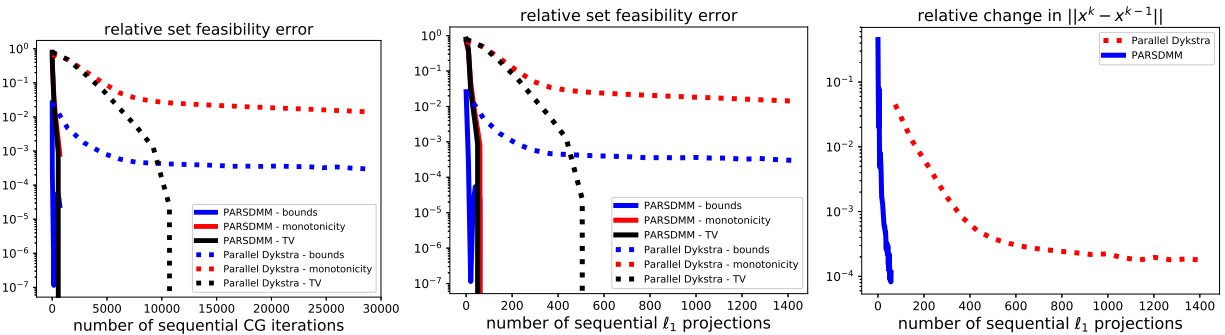


Figure 1: Relative transform-domain set feasibility (equation 26) as a function of the number of conjugate-gradient iterations and projections onto the 1-norm ball. This figure also shows relative change per iteration in the solution.

Because non-convex sets are an important application for us, we compare the performance for a non-convex intersection as well:

1. $\{m \mid \sigma_1 \leq m[i] \leq \sigma_2\}$: bound constraints
2. $\{m \mid (D_z \otimes I_x)m = \text{vec}(\sum_{j=1}^r \lambda[j]u_jv_j^\top)\}$, where $r < \min(n_z, n_x)$, $\lambda[j]$ are the singular values, and u_j, v_j are singular vectors: rank constraints on the vertical gradient of the image

We count the computational operations in the same way as in the previous example, but this time the computationally most costly projection is onto the set of matrices with limited rank via the singular value decomposition. The results in Figure 2 show that the convergence of parallel Dykstra’s algorithm almost stalls: the solution estimate gets closer to satisfying the bound constraints, but there is hardly any progress towards the rank constraint set. PARSDMM does not seem to struggle with the non-convex set in this particular example.

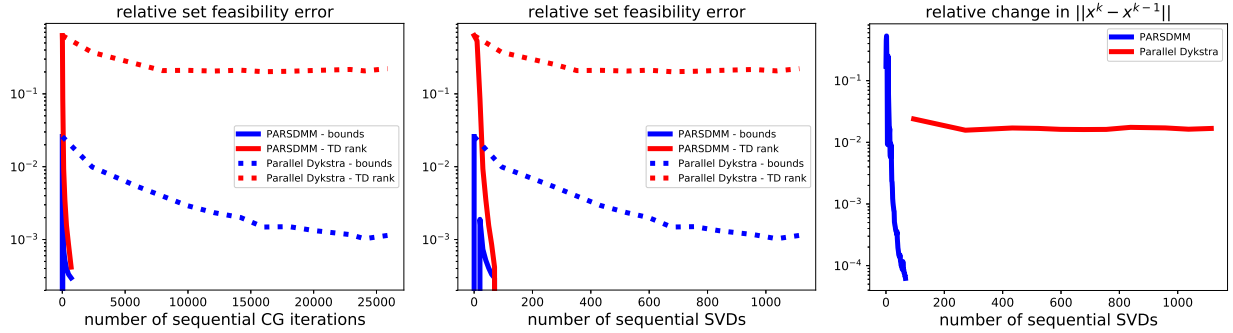


Figure 2: Relative transform-domain set feasibility (equation 26) as a function of the number of conjugate-gradient iterations and projections onto the set of matrices with limited rank via the SVD. This figure also shows relative change per iteration in the solution.

We used the single-level version of PARSDMM such that we can compare the computational cost with Parallel Dykstra. The PARSDMM results in this section are therefore pessimistic in general, as the multilevel version can offer additional speedups, which we show next.

Timings for 2D and 3D projections

To get an idea about solution times versus model size, as well as how beneficial the parallelism and multilevel continuation are, we show timings for projections of geological models onto an intersection for the four modes of operation: PARSDMM, parallel PARSDMM, multilevel PARSDMM, and multilevel parallel PARSDMM. As we mentioned, the multilevel version has a small additional overhead compared to single-level PARSDMM because of one interpolation procedure per level. Parallel PARSDMM has communication overhead. Note that serial PARSDMM still uses multi-threading for projections, the matrix-vector product in the conjugate-gradient method, and BLAS operations, but the y_i and v_i computations in Algorithm 1 remain sequential for every $i = 1, 2, \dots, p, p + 1$, contrary to parallel PARSDMM. We carry our computations out on a dedicated cluster node with 2 CPUs per node with 10 cores per CPU (Intel Ivy Bridge 2.8 GHz E5-2680v2) and 128 GB of memory per node.

The following sets are used in Peters et al. [2018] to regularize a geophysical inverse problem and form the intersection for our test case:

1. $\{m \mid \sigma_1 \leq m[i] \leq \sigma_2\}$: bound constraints

2. $\{m \mid -\sigma_3 \leq ((I_z \otimes D_x)m)[i] \leq \sigma_3\}$: lateral smoothness constraints. There are two of these constraints in the 3D case: for the x and y direction separately.
3. $\{m \mid 0 \leq ((D_z \otimes I_x)m)[i] \leq \infty\}$: vertical monotonicity constraints

The results in Figure 3 show that the multilevel strategy is much faster than the single-level version of PARSDMM. The multilevel overhead costs are thus small compared to the speedup. It also shows that, as expected, the parallel versions require some communication time, so the problems need to be large enough for the parallel version of PARSDMM to offer speedups.

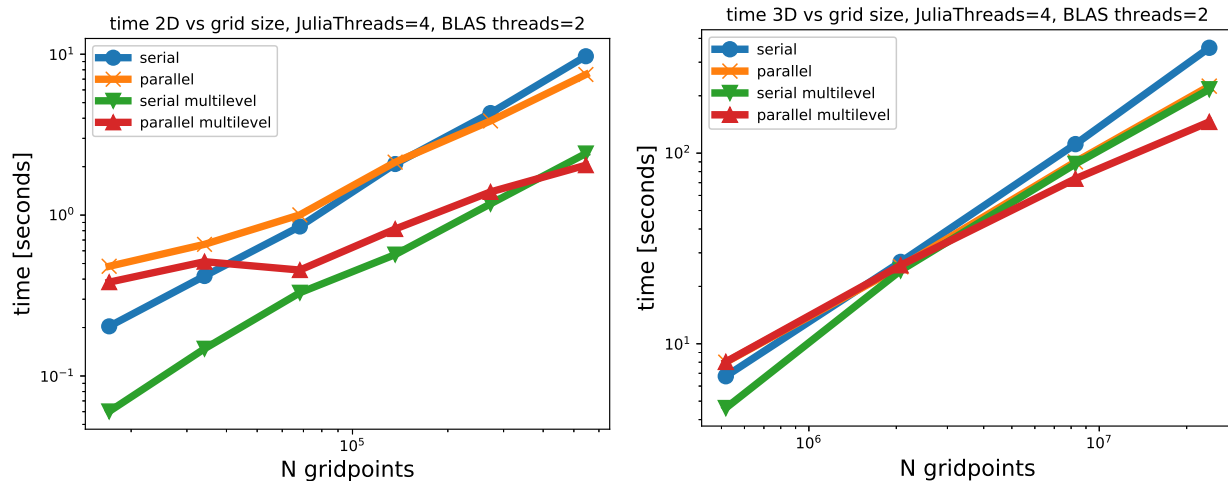


Figure 3: Timings for a 2D and 3D example where we project a geological model onto the intersection of bounds, lateral smoothness, and vertical monotonicity constraints.

Geophysical parameter estimation with constraints

Seismic full-waveform inversion (FWI) estimates rock properties (acoustic velocity in this example) from seismic (pressure) signals measured by hydrophones. FWI is a partial-differential-equation (PDE) constrained optimization problem where after eliminating the PDE constraint, the simulated data, $d_{\text{predicted}}(m)$, are connected nonlinearly to the unknown model parameters, $m \in \mathbb{R}^N$. We assume that we know the source and receiver locations, as well as the source function. A classic example of an objective for FWI is the nonlinear least-squares misfit $f(m) = 1/2 \|d_{\text{obs}} - d_{\text{predicted}}(m)\|_2^2$, which we use for this numerical experiment.

FWI is a problem hampered by local minima. Empirical evidence [Esser et al., 2018, Peters and Herrmann, 2017, Yong et al., 2018] suggests that we can mitigate issues with parasitic local minima by insisting that all model iterates be elements of the intersection of multiple constraint sets. This means that we add regularization to the objective $f(m) : \mathbb{R}^N \rightarrow \mathbb{R}$ in the form of multiple constraints—i.e., we have

$$\min_m f(m) \quad \text{s.t.} \quad m \in \mathcal{V} = \bigcap_{i=1}^p \mathcal{V}_i. \quad (29)$$

We use the spectral projected gradient (SPG) algorithm with a non-monotone line search [Birgin et al., 1999] to solve the above problem. SPG uses information from the current and previous gradient of $f(m)$

to approximate the action of the Hessian of $f(m^k)$ with the scalar α : the Barzilai-Borwein step length. At iteration k , SPG updates the model parameters as follows:

$$m^{k+1} = (1 - \gamma)m^k - \gamma\mathcal{P}_{\mathcal{V}}(m^k - \alpha\nabla_m f(m^k)), \quad (30)$$

where the non-monotone line search determines $\gamma \in (0, 1]$ and backtracks between two points in a convex set if all \mathcal{V}_i are convex. We compute the projection onto the intersection using PARSDMM (Algorithm 1). The total number of SPG iterations plus line-search steps is limited to the relatively small number of ten, because these require the solution of multiple PDEs, which is computationally intensive, especially in 3D.

The experimental setting is as follows: The Helmholtz equation models the wave propagation in an acoustic model. The data acquisition system is a vertical-seismic-profiling experiment with sources at the surface and receivers in a well, see Figure 4. All boundaries are perfectly-matched-layers (PML) that absorb outgoing waves as if the model is spatially unbounded. The challenges that we address by constraining the model parameters are: one-sided ‘source illumination’ that often leads to spurious artifacts in the source-receiver direction, a limited frequency range (3 – 10 Hertz), and the non-convexity of the data-misfit $f(m)$. We use the software by Da Silva and Herrmann [2017] to simulate seismic data and compute $f(m)$ and $\nabla_m f(m)$.

The prior knowledge consists of: (a) minimum and maximum velocities (2350 – 2650 m/s); (b) The anomaly is rectangular, but we do not know the size, aspect ratio, or location.

We start simple and look at what happens if we add bounds and total-variation constraints. Figure 4 shows the true model, initial guess, and the estimated models using convex constraints. The data acquisition geometry causes the model estimate with bound constraints to be an elongated diagonal anomaly that is incorrect in terms of size, shape, orientation, and parameter values. Figure 4(d) shows that even in the unusual case that we know and use an anisotropic total-variation (TV) constraint equal to the TV of the true model, we obtain a model estimate where the shape of the anomaly is still far from the truth, although many of the spurious oscillations are damped.

As we will demonstrate, the inclusion of multiple non-convex cardinality and rank constraints help the parameter estimation in this example. From the prior information that the anomaly is rectangular and aligned with the domain boundaries, we deduce that the rank of the model is equal to two. We also know that the cardinality of the discrete gradient of each row and each column is less than or equal to two as well. If we assume that the anomaly is not larger than half the total domain extent in each direction, we know that the cardinality of the discrete derivative of the model (in matrix format) is not larger than the number of grid points in each direction. To summarize, the following constraint sets follow from the prior information:

1. $\{x \mid \text{card}((D_z \otimes I_x)x) \leq n_x\}$
2. $\{x \mid \text{card}((I_z \otimes D_x)x) \leq n_z\}$
3. $\{x \mid \text{rank}(x) \leq 3\}$
4. $\{x \mid 2350 \leq x[i] \leq 2650 \forall i\}$
5. $\{x \mid \text{card}(D_x X[i, :]) \leq 2 \text{ for } i \in \{1, 2, \dots, n_z\}\}$, $X[i, :]$ is a row of the 2D model
6. $\{x \mid \text{card}(D_z X[:, j]) \leq 2 \text{ for } j \in \{1, 2, \dots, n_x\}\}$, $X[:, j]$ is a column of the 2D model

We use slightly overestimated rank and matrix cardinality constraints compared to the true model to mimic the more realistic situation that we typically have a priori access to over-estimated model properties. The results in Figure 5 use PARSDMM to compute projections onto the intersection of constraints, and show that non-convex constraints can lead to improved model estimates. Figure 5(a) is the result of working with constraints [1, 2, 3, 4], Figure 5(b) uses constraints [1, 2, 4, 5, 6], and Figure 5(c) uses all constraints [1, 2, 3, 4, 5, 6]. The result with rank constraints and both matrix and row/column-based cardinality constraints on the discrete gradient of the model is the most accurate in terms of the recovered anomaly shape. All results in Figure 4 that work with non-convex sets are at least as accurate as the result obtained with the true TV in terms of anomaly shape. Another important observation is that all non-convex results estimate a

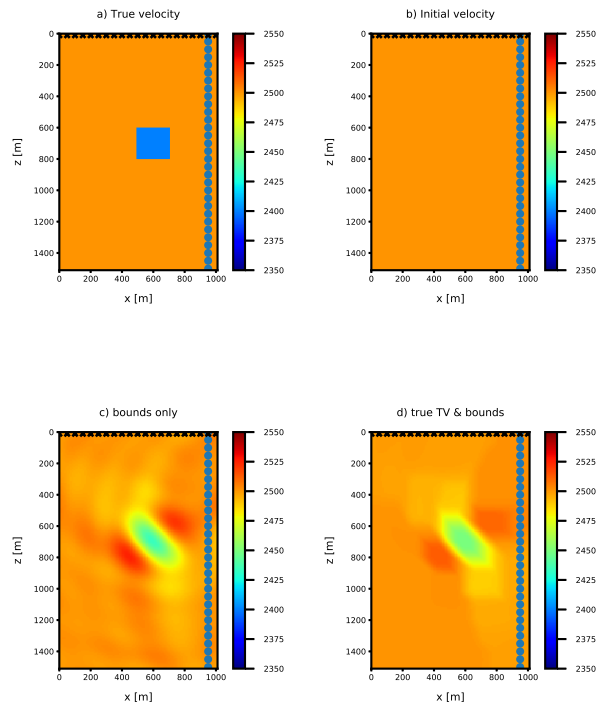


Figure 4: True, initial, and estimated models with convex constraints for the full-waveform inversion example. Crosses and circles represent sources and receivers, respectively. All projections inside the spectral projected gradient algorithm are computed using PARSDMM.

lower-than-background velocity anomaly, although not as low as the true anomaly. Contrary, the models obtained using convex sets show incorrect higher-than-background velocity artifacts in the vicinity of the true anomaly location.

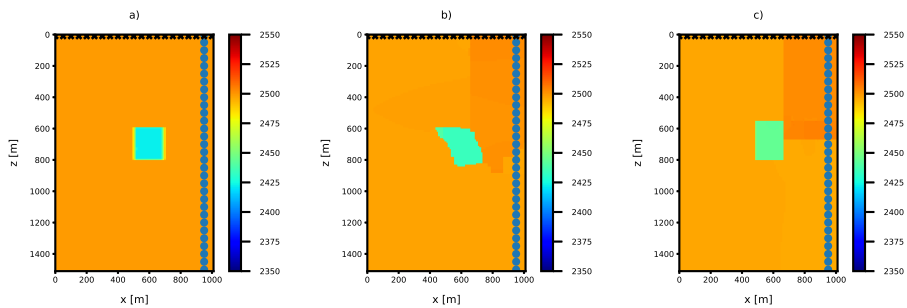


Figure 5: FWI results using various combinations of convex and non-convex constraints using PARSDMM.

Learning a parametrized intersection from a few training examples

In the introduction, we discussed projection or feasibility problem (4) formulations of inverse problems. The PARSDMM algorithm (15) is a good candidate to solve these types of problems because we mitigate rapidly increasing computation times for problems with many sets, by taking the similarity between linear operators in set definitions into account. Of course, we can only use multiple constraint sets if we have multiple pieces of prior information. Combettes and Pesquet [2004] present a simple solution and note that for 15 out of 20 investigated data-sets, 99% of the images have a total-variation within 20% of the average total variation of the data-set. The average total-variation serves as a constraint set that typically leads to good results. Here we follow the same reasoning, but we will work with many constraint sets that we learn from a few example images. To summarize, our strategy is as follows:

1. Observe the constraint parameters in various transform-domains for all training examples (independently in parallel for each example and each constraint).
2. Add a data-fit constraint.
3. The solution of the inverse problem is the projection of an initial guess m onto the intersection of sets that describe model properties and data-fit

$$\min_{x, \{y_i\}} \frac{1}{2} \|x - m\|_2^2 + \sum_{i=1}^{p-1} \iota_{C_i}(y_i) + \iota_{C_p^{\text{data}}}(y_p) \quad \text{s.t.} \quad \begin{cases} A_i x = y_i \\ Fx = y_p \end{cases}, \quad (31)$$

where F is a linear forward modeling operator.

Before we proceed to the examples, it is worth mentioning the main advantages of this strategy. Because all set definitions are independent of all other sets, there are no penalty/weight parameters, and we avoid hand-tuning the constraint definitions. We can observe ‘good’ constraints from just one or a few example images. Methods that do not require training, such as basis-pursuit type formulations [e.g., Lustig et al., 2007, Candès and Recht, 2009, van den Berg and Friedlander, 2009, Becker et al., 2011, Aravkin et al., 2014], often minimize the ℓ_1 norm or nuclear norm of transform-domain coefficients (e.g., Fourier, wavelet) of an image subject to a data-fit constraint. However, without learning, these methods require hand picking a suitable transform for each class of images. We will work with many transform-domain operators simultaneously, so that at least some of the constraint/linear operator combinations will describe uncorrupted images with small norms/bounds/cardinality, but not noisy/blurred/masked images. Note that we are not learning any dictionaries, but work with pre-defined transforms such as the Fourier basis, wavelets, and linear operators based on discrete gradients.

For both of the next two examples we observe the following constraint parameters from exemplar images:

1. $\{m \mid \sigma_1 \leq m[i] \leq \sigma_2\}$ (upper and lower bounds)
2. $\{m \mid \sum_{j=1}^k \lambda[j] \leq \sigma_3\}$ with $m = \text{vec}(\sum_{j=1}^k \lambda[j] u_j v_j^\top)$ is the SVD of the image (nuclear norm)
3. $\{m \mid \sum_{j=1}^k \lambda[j] \leq \sigma_4\}$, with $(D_z \otimes I_x)m = \text{vec}(\sum_{j=1}^k \lambda[j] u_j v_j^*)$ is the SVD of the vertical derivative of the image (nuclear norm of discrete gradients of the image, total-nuclear-variation). Use similar constraint for the x-direction.
4. $\{m \mid \|Am\|_1 \leq \sigma_5\}$ with $A = \begin{pmatrix} D_z \otimes I_x \\ I_z \otimes D_x \end{pmatrix}$ (anisotropic total-variation)
5. $\{m \mid \sigma_6 \leq \|m\|_2 \leq \sigma_7\}$ (annulus)
6. $\{m \mid \sigma_8 \leq \|Am\|_2 \leq \sigma_9\}$ with $A = \begin{pmatrix} D_z \otimes I_x \\ I_z \otimes D_x \end{pmatrix}$ (annulus of the discrete gradients of the training images)
7. $\{m \mid \|Am\|_1 \leq \sigma_{10}\}$ with $A =$ discrete Fourier transform (ℓ_1 -norm of DFT coefficients)

8. $\{m \mid -\sigma_{11} \leq ((D_z \otimes I_x)m)[i] \leq \sigma_{12}\}$ (slope-constraints in the z -direction, bounds on the discrete gradients of the image). Use similar constraint for the x -direction.
9. $\{m \mid \|Am\|_1 \leq \sigma_{11}\}$ with $A =$ discrete wavelet transform

These are nine types of convex and non-convex constraints on the model properties (11 sets passed to PARSDMM because sets three and eight are applied to the two directions separately). For data-fitting, we add a point-wise constraint, $\{x \mid l \leq (Fx - d_{\text{obs}}) \leq u\}$ with a linear forward model $F \in \mathbb{R}^{M \times N}$.

Joint deblurring-denoising-inpainting

The goal of the first example is to recover a $[0 - 255]$ grayscale image from 20% observed pixels of a blurred image (25 pixels known motion blur), where each observed data point also contains zero-mean random noise in the interval $[-10 - 10]$. The forward operator F is thus a restriction of an averaging matrix. As an additional challenge, we do not assume exact knowledge of the noise level and work with the over-estimation $[-15 - 15]$. The data set contains a series of images from ‘Planet Labs PlanetScope Ecuador’ with a resolution of three meters, available at openaerialmap.org. There are 35 patches of 1100×1100 pixels for training, some of which are displayed in Figure 6.

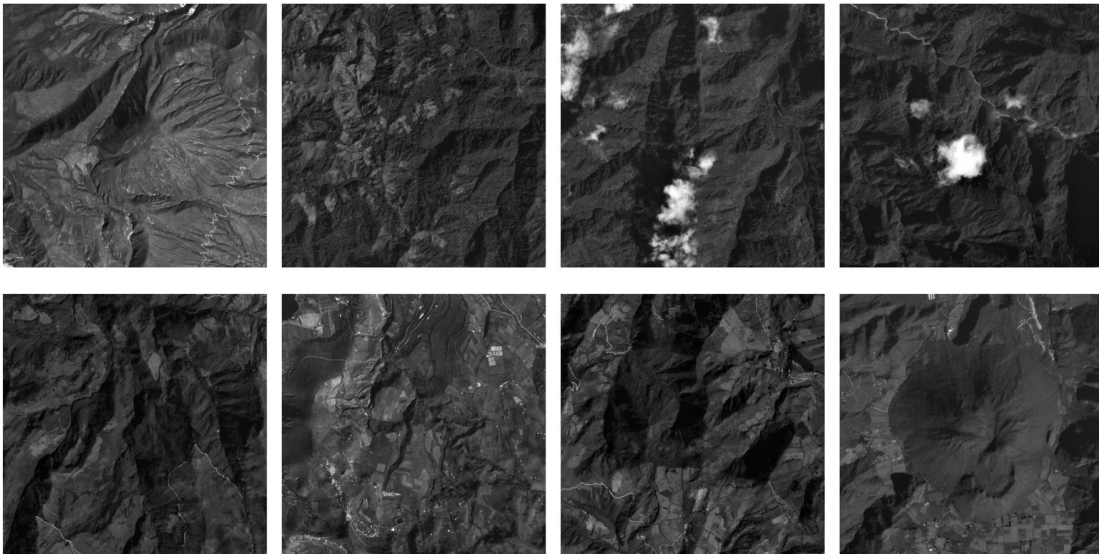


Figure 6: A sample of 8 out of 35 training images.

We compare the results of the projection onto the intersection of the 11 learned constraints using the proposed PARSDMM algorithm, to a basis pursuit denoise (BPDN) formulation that recovers a vector of wavelet coefficients, c , by solving $\min_c \|c\|_1$ s.t. $\|FW^*c - d_{\text{obs}}\|_2 \leq \sigma$ (BPDN-wavelet). The matrix W represents the wavelet transform: Daubechies Wavelets as implemented by the SPOT linear operator toolbox (<http://www.cs.ubc.ca/labs/scl/spot/index.html>) and computed with the Rice Wavelet Toolbox (RWT, github.com/ricedsp/rwt). We solve BPDN-wavelet using the SPGL1 algorithm [van den Berg and Friedlander, 2009].

In Figure 7 we see that an overestimation of σ in the BPDN formulation results in oversimplified images, because the ℓ_2 -ball constraint is too large which leads to a coefficient vector c that has an ℓ_1 norm that is

small compared to the true image. The values for l and u in the data-fit constraint $\{x \mid l \leq (Fx - d_{\text{obs}}) \leq u\}$ are also too large. However, the results from the projection onto the intersection of multiple constraints suffer much less from overestimated noise levels, because there are many other constraints that control the model properties. The results in Figure 7 show that the learned set-intersection approach achieves a higher PSNR for all evaluation images compared to the BPDN formulation.

Image desaturation

To illustrate the versatility of the learning strategy, algorithm, and constraint sets from the previous example, we now solve an image desaturation problem for a different data set. The only two things that we change are the constraint set parameters, which we observe from new training images (Figure 8), and a different linear forward operator F . The data set contains image patches (1500×1250 pixels) from the ‘Desa Sangaji Kota Ternate’ image with a resolution of 11 centimeters, available at openaerialmap.org. The corrupted observed images are saturated grayscale and generated by clipping the pixel values from $0 - 60$ to 60 and from $125 - 255$ to 125 , so there is saturation on both the dark and bright pixels. If we have no other information about the pixels at the clipped value, the desaturation problem implies the point-wise bound constraints [e.g., Mansour et al., 2010]

$$\begin{cases} 0 \leq x[i] \leq 60 & \text{if } d^{\text{obs}}[i] = 60 \\ x[i] = d^{\text{obs}}[i] & \text{if } 60 < d^{\text{obs}}[i] < 125 . \\ 125 \leq x[i] \leq 255 & \text{if } d^{\text{obs}}[i] = 125 \end{cases} \quad (32)$$

The forward operator is thus the identity matrix. We solve problem (31) with these point-wise data-fit constraints and the 11 model-property constraints listed earlier.

Figure 9 shows the results, true and observed data for four evaluation images. Large saturated patches are not desaturated accurately everywhere, because they contain no non-saturated observed pixels that serve as ‘anchor’ points.

Both the desaturation and the joint deblurring-denoising-inpainting example show that PARSDMM with multiple convex and non-convex sets converges to good results, while only a few training examples were sufficient to estimate the constraint set parameters. Because of the problem formulation, algorithms, and simple learning strategy, there were no parameters to hand-pick.

Discussion and future research directions

We developed algorithms to compute projections onto intersections of multiple sets that help setting up and solving constrained inverse problems. Our design choices, together with the constrained formulation, minimize the number of parameters that we need to hand-pick for the problem formulation, algorithms, and regularization. Our software package `SetIntersectionProjection` helps inverse problem practitioners to test various combinations of constraints for faster evaluation of their strategies to solve inverse problems. Besides practicality, we want our work to apply not just toy problems, but also to models on larger 3D grids. We achieved this via automatic adjustment of scalar algorithm parameters, parallel implementation, and multilevel acceleration. There are some limitations, but also opportunities to increase computational performance that we will now discuss.

Regarding the scope of the `SetIntersectionProjection` software, we emphasize that satisfying a constraint for our applications in imaging inverse problems is different from solving general (non-convex) optimization problems. When we refer to ‘reliably’ solving a non-convex problem, we are satisfied with an algorithm that usually approximates the solution well. For example, if we seek to image a model m that has k discontinuities, we add the constraint $\{m \mid \text{card}(Dm) \leq k\}$ where D is a derivative operator. A satisfying solution for our

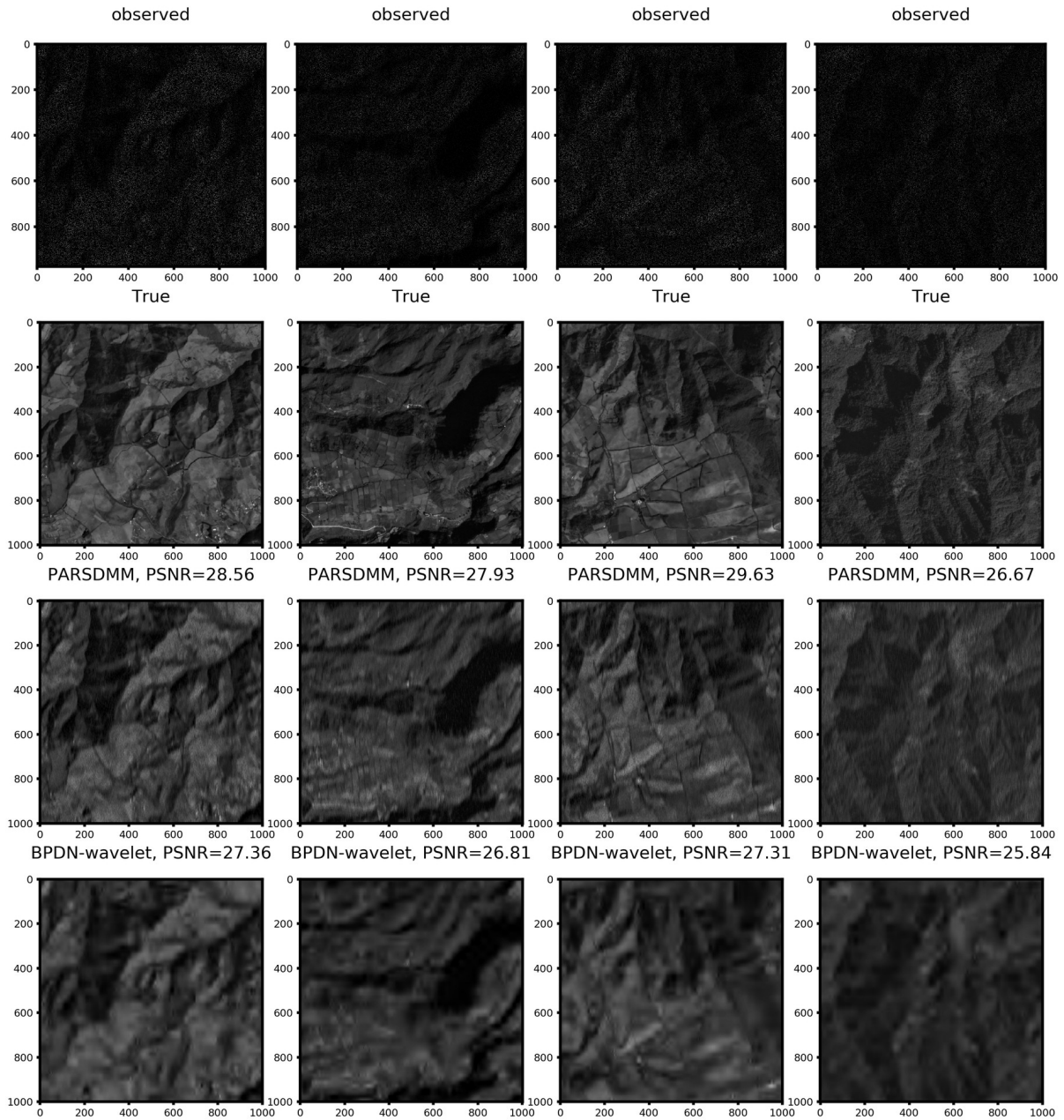


Figure 7: Reconstruction results from 80% missing pixels of an image with motion blur (25 pixels) and zero-mean random noise in the interval $[-10, 10]$. Results that are the projection onto an intersection of multiple learned constraints sets with PARSDMM are visually better than the BPDN-wavelet results.

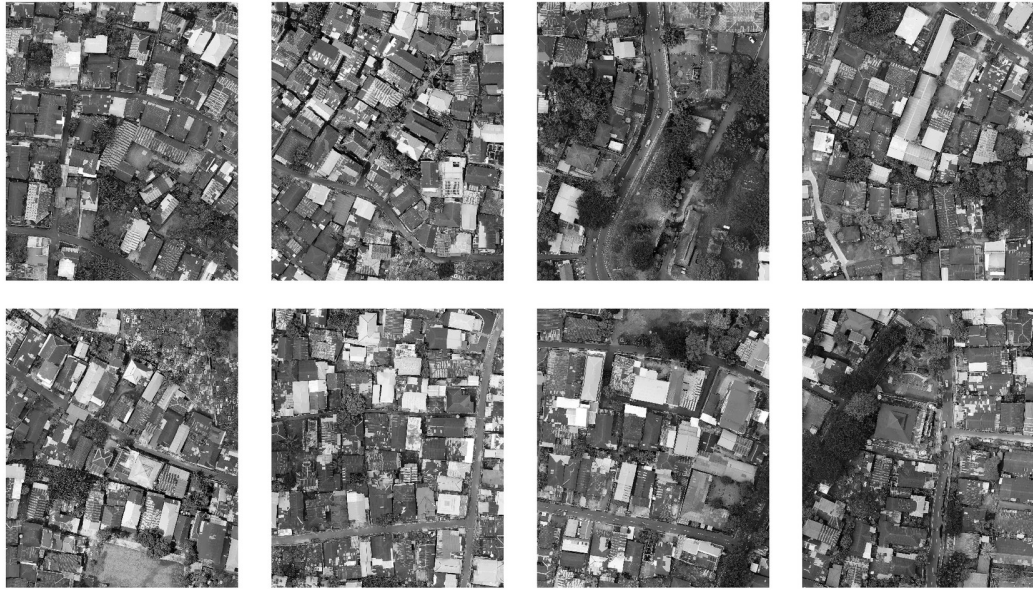


Figure 8: A sample of 8 out of 16 training images.

applications has k large vector entries, whereas all others are small. We do not need to find a vector that has a cardinality of exactly k , because the estimated model is the same for practical purposes if the results are assessed qualitatively, or where the expected resolution is much lower than the fine details we could potentially improve. Moreover, the forward operator for the inverse problem often is not sensitive to small changes in the model, and we do not benefit from spending much more computational time trying to find a more accurate solution to the non-convex problem. Besides the multilevel projection and automatic adjustment of augmented-Lagrangian parameters that we already use, [Diamond et al., 2018] present several other heuristics that can improve the solution of non-convex problems in the context of ADMM-based algorithms. Future work could test if these heuristics are computationally feasible for our often large-scale problems and if they cooperate with our other heuristics.

Besides the limitations and scope of this work, we highlight two ways how we can reduce computation times for Algorithm 1 and its multilevel version. First, we recognize that our algorithms use ADMM as its foundation, which is a synchronous algorithm. This means that the computations of the projections (y -update) in parallel are as slow as the most time-consuming projection. Without fundamentally changing the algorithms to asynchronous or randomized projection methods, we can take a purely software-based approach. Because we compute projections in parallel, where each projection uses several threads, we are free to reallocate threads from the fastest projection to the slowest and reduce the total computational time.

A second computational component that may be improved is the inexact linear system solve with the conjugate-gradient (CG) method. We do not use a preconditioner at the moment. Preliminary tests with a simple diagonal (Jacobi) preconditioner or multigrid V-cycle did reduce the number of CG iterations, but not the running time for CG in general. There are a few challenges we face when we design a preconditioner: *(i)* users may select a variety of linear operators *(ii)* the system matrix is the weighted sum of multiple linear systems in normal equation form *(iii)* the weights may change every two PARSDMM iterations *(iv)* the

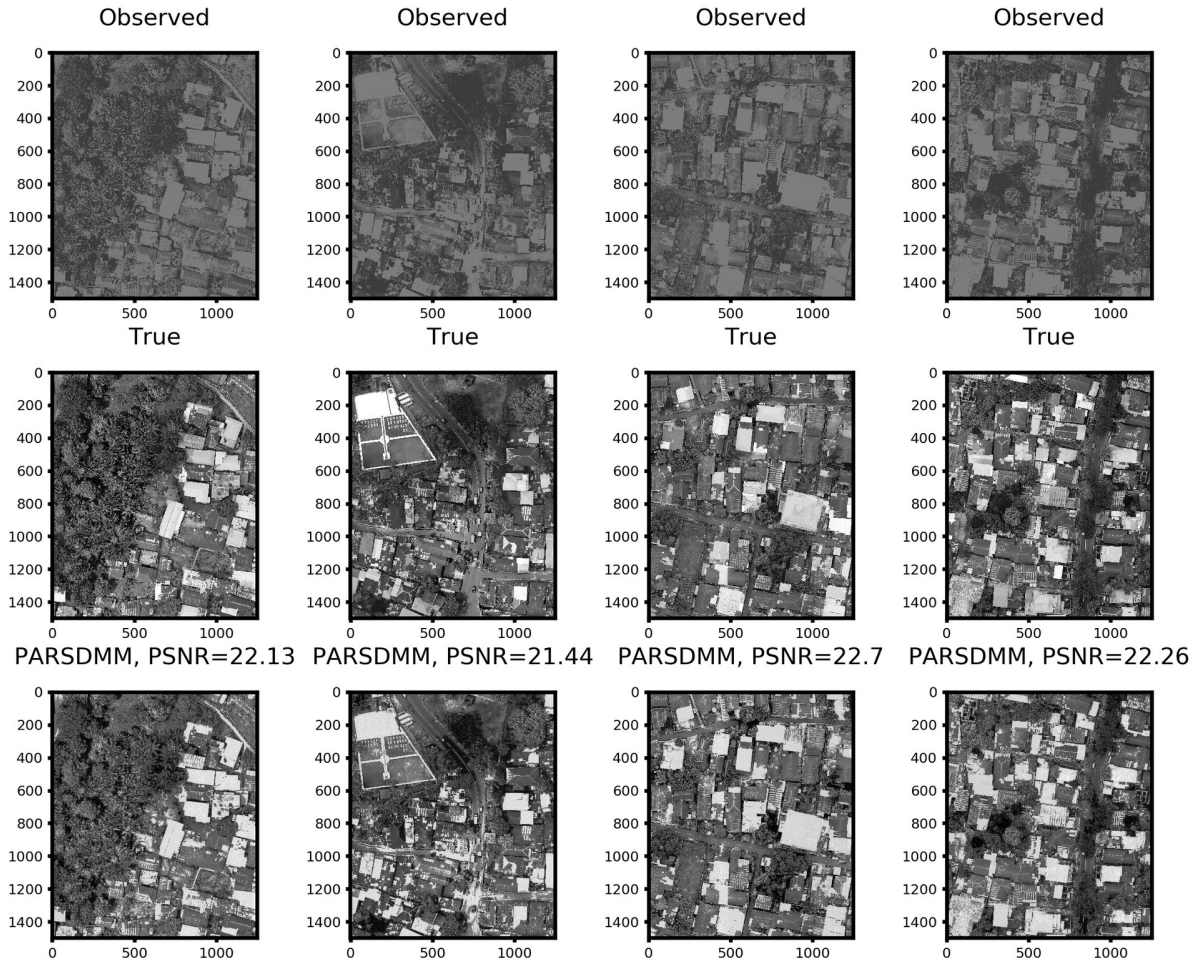


Figure 9: Reconstruction results from recovery from saturated images as the projection onto the intersection of 12 constraint sets.

number of CG iterations varies per PARSDMM iteration and is often less than ten, which makes it difficult for preconditioners to reduce the time consumption if they require some computational overhead or setup time.

Finally we mention how our software package can work cooperatively with recent developments in plug-and-play regularizers [Venkatakrishnan et al., 2013]. The general idea is to use black-box image processing techniques such as pre-trained neural networks [Zhang et al., 2017, Bigdeli and Zwicker, 2017, Fan et al., 2017, Chang et al., 2017, Aggarwal et al., 2018, Buzzard et al., 2018], as a map $g(x) : \mathbb{R}^N \rightarrow \mathbb{R}^N$ that behaves like a proximal operator or projector. Despite the fact that these plug-and-play algorithms do not, in general, share non-expansiveness properties with projectors [Chan et al., 2017], they are successfully employed in optimization algorithms based on operator-splitting. In our case, we can use a neural network as the projection operator with the identity matrix as associated linear operator. In this way we combine data-constraints and other prior information with a network. A potential challenge with the plug-and-play concept for constrained optimization is the difficulty to verify that the intersection of constraints is effectively non-empty, i.e., can $g(x)$ map to points in the intersection of the other constraint sets? Some preliminary

tests showed encouraging results and we intent to explore this line of research further.

Conclusions

We developed novel algorithms and corresponding software, the `SetIntersectionProjection` package, for the computation of projections onto the intersection of multiple constraint sets. These intersection projections are an important tool for the regularization of inverse problems. They may be used as the projection part of projected gradient/(quasi-)Newton algorithms. Projections onto an intersection also solve set-based formulations for linear image processing problems, possibly combined with simple learning techniques to extract set definitions from example images. The algorithms focus on problems with multiple sets for which we may not have closed-form projections. We enhance the computational performance for small 2D up to larger 3D models by specializing the software for projection problems, exploiting different levels of parallelism on multi-core computing platforms, automatic selection of scalar (acceleration) parameters, and a coarse-to-fine grid multilevel implementation. The software is practical, also for non-expert users, because we do not need manual step-size selection or related operator norm computations and the algorithm inputs are pairs of linear operators and projectors, which the software also generates. Another practical feature is the support for simultaneous set definitions based on the entire image/tensor and each slice/row/column. Because we focus on multiple constraints, there is less of a need to choose the ‘best’ constraint with the ‘best’ linear operator/transform for a given inverse problem. More constraints are not much more difficult to deal with than a one or two constraints, also in terms of computational cost per iteration. We demonstrated the versatility of the presented algorithms and software using examples from partial-differential-equation based parameter estimation and image processing. These examples also show that the algorithms perform well on problems that include non-convex sets.

Appendix A: Black-box alternating projection methods

We briefly show that the proposed PARSDMM algorithm (Algorithm 1) is different, but closely related to black-box alternating projection algorithms for computing the projection onto an intersection of sets. We base this appendix on the alternating direction method of multipliers (ADMM). The ADMM algorithm is closely related to Dykstra’s algorithm [Dykstra, 1983, Boyle and Dykstra, 1986] for projection problems, as described by [Bauschke and Koch, 2015, Tibshirani, 2017], including the conditions that lead to equivalency.

The parallel version of Dykstra’s algorithm (Algorithm 4) projects the vector $m \in \mathbb{R}^N$ onto an intersection of p sets using projections onto each set separately using projectors $\mathcal{P}_{\mathcal{V}_1}, \mathcal{P}_{\mathcal{V}_2}, \dots, \mathcal{P}_{\mathcal{V}_p}$. If the definitions of the sets \mathcal{V}_i include non-orthogonal linear operators, these projections are often non-trivial and their computation requires another iterative algorithm.

To show the similarity and difference between PARSDMM and parallel Dykstra’s algorithm, we proceed with a derivation similar to Algorithm 1, but different in such a way that the final algorithm is black-box, i.e., it uses projections onto the sets \mathcal{V}_i and the linear operators are ‘hidden’.

First we rewrite the projection problem of m onto the intersection of sets \mathcal{V}_i ,

$$\min_x \frac{1}{2} \|x - m\|_2^2 + \sum_{i=1}^{p-1} \iota_{\mathcal{V}_i}(x) \quad (33)$$

as

$$\min_x \frac{1}{2} \|x - m\|_2^2 + \sum_{i=1}^{p-1} \iota_{\mathcal{C}_i}(A_i x). \quad (34)$$

Algorithm 4 Parallel Dykstra's algorithm to compute $\arg \min_x \frac{1}{2} \|x - m\|_2^2$ s.t. $x \in \bigcap_{i=1}^p \mathcal{V}_i$.

Algorithm Parallel-DYKSTRA($m, \mathcal{P}_{\mathcal{V}_1}, \mathcal{P}_{\mathcal{V}_2}, \dots, \mathcal{P}_{\mathcal{V}_p}$)

input:

model to project: m

projectors onto sets $\mathcal{P}_{\mathcal{V}_1}, \mathcal{P}_{\mathcal{V}_2}, \dots, \mathcal{P}_{\mathcal{V}_p}$

//initialize

0a. $x^0 = m, k = 1$

0b. $v_i^0 = x^0$ for $i = 1, 2, \dots, p$

0c. select weights ρ_i such that $\sum_{i=1}^p \rho_i = 1$

while stopping conditions not satisfied **do**

FOR $i = 1, 2, \dots, p$

1. $y_i^{k+1} = \mathcal{P}_{\mathcal{V}_i}(v_i^k)$

END

2. $x^{k+1} = \sum_{i=1}^p \rho_i y_i^{k+1}$

FOR $i = 1, 2, \dots, p$

3. $v_i^{k+1} = x^{k+1} + v_i^k - y_i^{k+1}$

END

4. $k \leftarrow k + 1$

END

output: x

Where we exposed linear operators A_i by rewriting the indicator functions $\iota_{\mathcal{V}_i}(x) \rightarrow \iota_{C_i}(A_i x)$. Now we introduce additional variables and equality constraints to set up a parallel algorithm as

$$\min_{x, \{y_i\}} \frac{1}{2} \|y_p - m\|_2^2 + \sum_{i=1}^{p-1} \iota_{C_i}(A_i y_i) \quad \text{s.t.} \quad x = y_i \quad \forall i. \quad (35)$$

This problem is suitable for solving with ADMM if we recast it as

$$\min_{x, \tilde{y}} \tilde{f}(\tilde{A} \tilde{y}) \quad \text{s.t.} \quad \tilde{D} x = \tilde{y}, \quad (36)$$

with

$$\tilde{f}(\tilde{y}) \equiv \frac{1}{2} \|y_p - m\|_2^2 + \sum_{i=1}^{p-1} \iota_{C_i}(A_i y_i) \quad (37)$$

and

$$\tilde{D} \equiv \begin{pmatrix} I_1 \\ \vdots \\ I_p \end{pmatrix}, \quad \tilde{y} \equiv \begin{pmatrix} y_1 \\ \vdots \\ y_p \end{pmatrix}, \quad \tilde{A} \equiv \begin{pmatrix} A_1 \\ \vdots \\ A_p \end{pmatrix}. \quad (38)$$

The linear equality constraints enforce that all y_i are copies of x at the solution of problem (35). The difference with PARSDMM is that we leave the A_i inside the indicator functions instead of moving them to the linear equality constraints. The corresponding augmented Lagrangian with penalty parameters $\rho_i > 0$ is

$$L_{\rho_1, \dots, \rho_p}(x, y_1, \dots, y_p, v_1, \dots, v_p) = \sum_{i=1}^p \left[\tilde{f}_i(A_i y_i) + v_i^\top (y_i - x) + \frac{\rho_i}{2} \|y_i - x\|_2^2 \right]. \quad (39)$$

The ADMM iterations with a relaxation parameters γ_i are then given by

$$\begin{aligned}
x^{k+1} &= \arg \min_x \sum_{i=1}^p \left[\frac{\rho_i^k}{2} \|y_i^k - x + \frac{v_i^k}{\rho_i^k}\|_2^2 \right] \\
&= \frac{\sum_{i=1}^p [\rho_i^k y_i^k + v_i^k]}{\sum_{i=1}^p \rho_i^k} \\
\bar{x}_i^{k+1} &= \gamma_i^k x_i^{k+1} + (1 - \gamma_i^k) y_i^k \\
y_i^{k+1} &= \arg \min_{y_i} \left[f_i(A_i y_i) + \frac{\rho_i}{2} \|y_i - \bar{x}_i^{k+1} + \frac{v_i^k}{\rho_i^k}\|_2^2 \right] \\
&= \text{prox}_{f_i \circ A_i, \rho_i^k} \left(\bar{x}_i^{k+1} - \frac{v_i^k}{\rho_i^k} \right) \\
v_i^{k+1} &= v_i^k + \rho_i^k (y_i^{k+1} - \bar{x}_i^{k+1}).
\end{aligned}$$

The difference with Algorithm 1 is that the linear operators A_i move from the x^{k+1} computation to the y_i^{k+1} computation. This means the x^{k+1} computation is now a simple averaging step instead of a linear system solution. The y_i^{k+1} changed from evaluating proximal maps (almost always in closed-form), into evaluations of proximal maps involving linear operators (usually not known in closed-form). The proximal maps $\text{prox}_{f_i \circ A_i, \rho_i^k}$ for $i = 1, \dots, p-1$ are projections onto \mathcal{V}_i , except for $i = p$, which is the proximal map for $\frac{1}{2} \|y_p - m\|_2^2$. We need another iterative algorithm to compute the y_i^{k+1} at relatively high computation cost. The algorithm as a whole becomes more complicated, because we need additional stopping criteria for the algorithm that computes the y_i updates.

This iterations from (40) are similar to parallel Dykstra (Algorithm 4) and are, in essence, ADMM applied to a standard consensus form optimization problem [Boyd et al., 2011, problem 7.1].

References

- M. V. Afonso, J. M. Bioucas-Dias, and M. A. T. Figueiredo. An augmented lagrangian approach to the constrained optimization formulation of imaging inverse problems. *IEEE Transactions on Image Processing*, 20(3):681–695, March 2011. ISSN 1057-7149. doi: 10.1109/TIP.2010.2076294.
- H. K. Aggarwal, M. P. Mani, and M. Jacob. Model based image reconstruction using deep learned priors (modl). In *2018 IEEE 15th International Symposium on Biomedical Imaging (ISBI 2018)*, pages 671–674, April 2018. doi: 10.1109/ISBI.2018.8363663.
- N. Antonello, L. Stella, P. Patrinos, and T. van Waterschoot. Proximal Gradient Algorithms: Applications in Signal Processing. *ArXiv e-prints*, Mar. 2018.
- F. J. Aragón Artacho and R. Campoy. A new projection method for finding the closest point in the intersection of convex sets. *Computational Optimization and Applications*, 69(1):99–132, Jan 2018. ISSN 1573-2894. doi: 10.1007/s10589-017-9942-5. URL <https://doi.org/10.1007/s10589-017-9942-5>.
- A. Aravkin, R. Kumar, H. Mansour, B. Recht, and F. J. Herrmann. Fast methods for denoising matrix completion formulations, with applications to robust seismic data interpolation. *SIAM Journal on Scientific Computing*, 36(5):S237–S266, 2014. doi: 10.1137/130919210. URL <https://doi.org/10.1137/130919210>.
- A. Y. Aravkin, J. V. Burke, D. Drusvyatskiy, M. P. Friedlander, and S. Roy. Level-set methods for convex optimization. *arXiv preprint arXiv:1602.01506*, 2016.

- U. M. Ascher and E. Haber. Grid refinement and scaling for distributed parameter estimation problems. *Inverse Problems*, 17(3):571–590, may 2001. doi: 10.1088/0266-5611/17/3/314. URL <https://doi.org/10.1088%2F0266-5611%2F17%2F3%2F314>.
- J. Barzilai and J. M. Borwein. Two-point step size gradient methods. *IMA Journal of Numerical Analysis*, 8(1):141–148, 1988. doi: 10.1093/imanum/8.1.141. URL <http://imajna.oxfordjournals.org/content/8/1/141.abstract>.
- H. H. Bauschke and V. R. Koch. Projection methods: Swiss army knives for solving feasibility and best approximation problems with halfspaces. *Contemporary Mathematics*, 636:1–40, 2015.
- A. Beck. *First-Order Methods in Optimization*. Society for Industrial and Applied Mathematics, Philadelphia, PA, 2017. doi: 10.1137/1.9781611974997. URL <http://epubs.siam.org/doi/abs/10.1137/1.9781611974997>.
- S. R. Becker, E. J. Candès, and M. C. Grant. Templates for convex cone problems with applications to sparse signal recovery. *Mathematical Programming Computation*, 3(3):165, Jul 2011. ISSN 1867-2957. doi: 10.1007/s12532-011-0029-5. URL <https://doi.org/10.1007/s12532-011-0029-5>.
- D. P. Bertsekas. Projected newton methods for optimization problems with simple constraints. *SIAM Journal on Control and Optimization*, 20(2):221–246, 1982. doi: 10.1137/0320018. URL <https://doi.org/10.1137/0320018>.
- J. Bezanson, A. Edelman, S. Karpinski, and V. B. Shah. Julia: A fresh approach to numerical computing. *SIAM Review*, 59(1):65–98, 2017. doi: 10.1137/141000671. URL <https://doi.org/10.1137/141000671>.
- S. A. Bigdeli and M. Zwickner. Image restoration using autoencoding priors. *arXiv preprint arXiv:1703.09964*, 2017.
- E. G. Birgin, J. M. Martínez, and M. Raydan. Nonmonotone spectral projected gradient methods on convex sets. *SIAM J. on Optimization*, 10(4):1196–1211, Aug. 1999. ISSN 1052-6234. doi: 10.1137/S1052623497330963. URL <http://dx.doi.org/10.1137/S1052623497330963>.
- S. Boyd, N. Parikh, E. Chu, B. Peleato, and J. Eckstein. Distributed optimization and statistical learning via the alternating direction method of multipliers. *Found. Trends Mach. Learn.*, 3(1):1–122, Jan. 2011. ISSN 1935-8237. doi: 10.1561/22000000016. URL <http://dx.doi.org/10.1561/22000000016>.
- J. P. Boyle and R. L. Dykstra. *A Method for Finding Projections onto the Intersection of Convex Sets in Hilbert Spaces*, pages 28–47. Springer New York, New York, NY, 1986. ISBN 978-1-4613-9940-7. doi: 10.1007/978-1-4613-9940-7_3. URL http://dx.doi.org/10.1007/978-1-4613-9940-7_3.
- G. Buzzard, S. Chan, S. Sreehari, and C. Bouman. Plug-and-play unplugged: Optimization-free reconstruction using consensus equilibrium. *SIAM Journal on Imaging Sciences*, 11(3):2001–2020, 2018. doi: 10.1137/17M1122451. URL <https://doi.org/10.1137/17M1122451>.
- E. J. Candès and B. Recht. Exact matrix completion via convex optimization. *Foundations of Computational Mathematics*, 9(6):717, Apr 2009. ISSN 1615-3383. doi: 10.1007/s10208-009-9045-5. URL <https://doi.org/10.1007/s10208-009-9045-5>.
- Y. Censor. Computational acceleration of projection algorithms for the linear best approximation problem. *Linear Algebra and its Applications*, 416(1):111 – 123, 2006. ISSN 0024-3795. doi: <http://dx.doi.org/10.1016/j.laa.2005.10.006>. URL <http://www.sciencedirect.com/science/article/pii/S0024379505004891>.
- Y. Censor, T. Elfving, N. Kopf, and T. Bortfeld. The multiple-sets split feasibility problem and its applications for inverse problems. *Inverse Problems*, 21(6):2071, 2005.

- S. H. Chan, X. Wang, and O. A. Elgendy. Plug-and-play admm for image restoration: Fixed-point convergence and applications. *IEEE Transactions on Computational Imaging*, 3(1):84–98, March 2017. ISSN 2333-9403. doi: 10.1109/TCI.2016.2629286.
- J. H. R. Chang, C. Li, B. Póczos, and B. V. K. V. Kumar. One network to solve them all — solving linear inverse problems using deep projection models. In *2017 IEEE International Conference on Computer Vision (ICCV)*, pages 5889–5898, Oct 2017. doi: 10.1109/ICCV.2017.627.
- S. Chen, D. Donoho, and M. Saunders. Atomic decomposition by basis pursuit. *SIAM Review*, 43(1):129–159, 2001. doi: 10.1137/S003614450037906X. URL <https://doi.org/10.1137/S003614450037906X>.
- P. Combettes. The convex feasibility problem in image recovery. volume 95 of *Advances in Imaging and Electron Physics*, pages 155 – 270. Elsevier, 1996. doi: [https://doi.org/10.1016/S1076-5670\(08\)70157-5](https://doi.org/10.1016/S1076-5670(08)70157-5). URL <http://www.sciencedirect.com/science/article/pii/S1076567008701575>.
- P. L. Combettes. The foundations of set theoretic estimation. *Proceedings of the IEEE*, 81(2):182–208, Feb 1993. ISSN 0018-9219. doi: 10.1109/5.214546.
- P. L. Combettes and J. C. Pesquet. Image restoration subject to a total variation constraint. *IEEE Transactions on Image Processing*, 13(9):1213–1222, Sept 2004. ISSN 1057-7149. doi: 10.1109/TIP.2004.832922.
- P. L. Combettes and J.-C. Pesquet. Proximal splitting methods in signal processing. In H. H. Bauschke, R. S. Burachik, P. L. Combettes, V. Elser, D. R. Luke, and H. Wolkowicz, editors, *Fixed-Point Algorithms for Inverse Problems in Science and Engineering*, volume 49 of *Springer Optimization and Its Applications*, pages 185–212. Springer New York, 2011. ISBN 978-1-4419-9568-1. doi: 10.1007/978-1-4419-9569-8_10. URL http://dx.doi.org/10.1007/978-1-4419-9569-8_10.
- S. C. Constable, R. L. Parker, and C. G. Constable. Occam’s inversion: A practical algorithm for generating smooth models from electromagnetic sounding data. *GEOPHYSICS*, 52(3):289–300, 1987. doi: 10.1190/1.1442303. URL <http://dx.doi.org/10.1190/1.1442303>.
- C. Da Silva and F. J. Herrmann. A Unified 2D/3D Large Scale Software Environment for Nonlinear Inverse Problems. *ArXiv e-prints*, Mar. 2017.
- S. Diamond, R. Takapoui, and S. Boyd. A general system for heuristic minimization of convex functions over non-convex sets. *Optimization Methods and Software*, 33(1):165–193, 2018. doi: 10.1080/10556788.2017.1304548. URL <https://doi.org/10.1080/10556788.2017.1304548>.
- A. Domahidi, E. Chu, and S. Boyd. Ecos: An socp solver for embedded systems. In *Control Conference (ECC), 2013 European*, pages 3071–3076. IEEE, 2013.
- J. Duchi, S. Shalev-Shwartz, Y. Singer, and T. Chandra. Efficient projections onto the l_1 -ball for learning in high dimensions. pages 272–279, 2008.
- R. L. Dykstra. An algorithm for restricted least squares regression. *Journal of the American Statistical Association*, 78(384):837–842, 1983. doi: 10.1080/01621459.1983.10477029. URL <http://www.tandfonline.com/doi/abs/10.1080/01621459.1983.10477029>.
- J. Eckstein and D. P. Bertsekas. On the douglas—rachford splitting method and the proximal point algorithm for maximal monotone operators. *Mathematical Programming*, 55(1):293–318, Apr 1992. ISSN 1436-4646. doi: 10.1007/BF01581204. URL <https://doi.org/10.1007/BF01581204>.
- J. Eckstein and W. Yao. Understanding the convergence of the alternating direction method of multipliers: Theoretical and computational perspectives. *Pac. J. Optim. To appear*, 2015.
- E. Esser. Applications of lagrangian-based alternating direction methods and connections to split bregman. *CAM report*, 9:31, 2009.

- E. Esser, L. Guasch, F. J. Herrmann, and M. Warner. Constrained waveform inversion for automatic salt flooding. *The Leading Edge*, 35(3):235–239, 2016. doi: 10.1190/tle35030235.1. URL <http://dx.doi.org/10.1190/tle35030235.1>.
- E. Esser, L. Guasch, T. van Leeuwen, A. Y. Aravkin, and F. J. Herrmann. Total variation regularization strategies in full-waveform inversion. *SIAM Journal on Imaging Sciences*, 11(1):376–406, 2018. doi: 10.1137/17M111328X. URL <https://doi.org/10.1137/17M111328X>.
- K. Fan, Q. Wei, L. Carin, and K. A. Heller. An inner-loop free solution to inverse problems using deep neural networks. In I. Guyon, U. V. Luxburg, S. Bengio, H. Wallach, R. Fergus, S. Vishwanathan, and R. Garnett, editors, *Advances in Neural Information Processing Systems 30*, pages 2370–2380. Curran Associates, Inc., 2017. URL <http://papers.nips.cc/paper/6831-an-inner-loop-free-solution-to-inverse-problems-using-deep-neural-networks.pdf>.
- P. Farrell, D. Ham, S. Funke, and M. Rognes. Automated derivation of the adjoint of high-level transient finite element programs. *SIAM Journal on Scientific Computing*, 35(4):C369–C393, 2013. doi: 10.1137/120873558. URL <https://doi.org/10.1137/120873558>.
- M. Frigo and S. G. Johnson. The design and implementation of fftw3. *Proceedings of the IEEE*, 93(2):216–231, Feb 2005. ISSN 0018-9219. doi: 10.1109/JPROC.2004.840301.
- W. Gander. Least squares with a quadratic constraint. *Numerische Mathematik*, 36(3):291–307, Sep 1980. ISSN 0945-3245. doi: 10.1007/BF01396656. URL <https://doi.org/10.1007/BF01396656>.
- G. H. Golub and U. von Matt. Quadratically constrained least squares and quadratic problems. *Numerische Mathematik*, 59(1):561–580, Dec 1991. ISSN 0945-3245. doi: 10.1007/BF01385796. URL <https://doi.org/10.1007/BF01385796>.
- E. Haber. *Computational methods in geophysical electromagnetics*. SIAM, 2014.
- E. Haber, U. M. Ascher, and D. Oldenburg. On optimization techniques for solving nonlinear inverse problems. *Inverse Problems*, 16(5):1263–1280, Oct. 2000. ISSN 0266-5611. doi: 10.1088/0266-5611/16/5/309. URL <http://stacks.iop.org/0266-5611/16/i=5/a=309?key=crossref.98f435f9ee66231b63da02b10f82a60b>.
- F. Heide, S. Diamond, M. Nießner, J. Ragan-Kelley, W. Heidrich, and G. Wetzstein. Proximal: Efficient image optimization using proximal algorithms. *ACM Trans. Graph.*, 35(4):84:1–84:15, July 2016. ISSN 0730-0301. doi: 10.1145/2897824.2925875. URL <http://doi.acm.org/10.1145/2897824.2925875>.
- F. Iutzeler and J. M. Hendrickx. A generic online acceleration scheme for optimization algorithms via relaxation and inertia. *Optimization Methods and Software*, 0(0):1–23, 2017. doi: 10.1080/10556788.2017.1396601. URL <https://doi.org/10.1080/10556788.2017.1396601>.
- V. K. Ivanov, V. V. Vasin, and V. P. Tanana. *Theory of linear ill-posed problems and its applications*, volume 36. Walter de Gruyter, 2013.
- Z. Jia, X. Cai, and D. Han. Comparison of several fast algorithms for projection onto an ellipsoid. *Journal of Computational and Applied Mathematics*, 319:320 – 337, 2017. ISSN 0377-0427. doi: <https://doi.org/10.1016/j.cam.2017.01.008>. URL <http://www.sciencedirect.com/science/article/pii/S0377042717300122>.
- S. Kitic, L. Albera, N. Bertin, and R. Gribonval. Physics-driven inverse problems made tractable with cosparsity regularization. *IEEE Transactions on Signal Processing*, 64(2):335–348, Jan 2016. ISSN 1053-587X. doi: 10.1109/TSP.2015.2480045.
- H. Kotakemori, H. Hasegawa, T. Kajiyama, A. Nukada, R. Suda, and A. Nishida. Performance evaluation of parallel sparse matrix-vector products on sgi altix3700. *Lecture Notes in Computer Science*, 4315:153–166, 2008.

- N. Kukreja, M. Louboutin, F. Vieira, F. Luporini, M. Lange, and G. Gorman. Devito: Automated fast finite difference computation. In *2016 Sixth International Workshop on Domain-Specific Languages and High-Level Frameworks for High Performance Computing (WOLFHPC)*, pages 11–19, Nov 2016. doi: 10.1109/WOLFHPC.2016.06.
- A. Kundu, F. Bach, and C. Bhattacharyya. Convex optimization over intersection of simple sets: improved convergence rate guarantees via an exact penalty approach. *ArXiv e-prints*, Oct. 2017.
- W. López and M. Raydan. An acceleration scheme for dykstra’s algorithm. *Computational Optimization and Applications*, 63(1):29–44, Jan 2016. ISSN 1573-2894. doi: 10.1007/s10589-015-9768-y. URL <https://doi.org/10.1007/s10589-015-9768-y>.
- M. Louboutin, P. Witte, M. Lange, N. Kukreja, F. Luporini, G. Gorman, and F. J. Herrmann. Full-waveform inversion, part 2: Adjoint modeling. *The Leading Edge*, 37(1):69–72, 2018. doi: 10.1190/tle37010069.1. URL <https://doi.org/10.1190/tle37010069.1>.
- M. Lustig, D. Donoho, and J. M. Pauly. Sparse mri: The application of compressed sensing for rapid mr imaging. *Magnetic Resonance in Medicine*, 58(6):1182–1195, 2007. ISSN 1522-2594. doi: 10.1002/mrm.21391. URL <http://dx.doi.org/10.1002/mrm.21391>.
- J. Macdonald and L. Ruthotto. Improved susceptibility artifact correction of echo-planar mri using the alternating direction method of multipliers. *Journal of Mathematical Imaging and Vision*, 60(2):268–282, Feb 2018. ISSN 1573-7683. doi: 10.1007/s10851-017-0757-x. URL <https://doi.org/10.1007/s10851-017-0757-x>.
- S. Mallat and Z. Zhang. Adaptive time-frequency decomposition with matching pursuits. In *[1992] Proceedings of the IEEE-SP International Symposium on Time-Frequency and Time-Scale Analysis*, pages 7–10, Oct 1992. doi: 10.1109/TFTSA.1992.274245.
- H. Mansour, R. Saab, P. Nasiopoulos, and R. Ward. Color image desaturation using sparse reconstruction. In *2010 IEEE International Conference on Acoustics, Speech and Signal Processing*, pages 778–781, March 2010. doi: 10.1109/ICASSP.2010.5494984.
- S. G. Nash. A multigrid approach to discretized optimization problems. *Optimization Methods and Software*, 14(1-2):99–116, 2000. doi: 10.1080/10556780008805795. URL <https://doi.org/10.1080/10556780008805795>.
- S. G. Nash. Properties of a class of multilevel optimization algorithms for equality-constrained problems. *Optimization Methods and Software*, 29(1):137–159, 2014. doi: 10.1080/10556788.2012.759571. URL <https://doi.org/10.1080/10556788.2012.759571>.
- R. Nishihara, L. Lessard, B. Recht, A. Packard, and M. I. Jordan. A general analysis of the convergence of admm. In *Int. Conf. Mach. Learn.*, volume 37, pages 343–352, 2015.
- J. Nocedal and S. J. Wright. *Numerical optimization*. Springer, 2000.
- B. O’Donoghue, E. Chu, N. Parikh, and S. Boyd. Conic optimization via operator splitting and homogeneous self-dual embedding. *Journal of Optimization Theory and Applications*, 169(3):1042–1068, Jun 2016. ISSN 1573-2878. doi: 10.1007/s10957-016-0892-3. URL <https://doi.org/10.1007/s10957-016-0892-3>.
- C. C. Paige and M. A. Saunders. Lsqr: An algorithm for sparse linear equations and sparse least squares. *ACM Trans. Math. Softw.*, 8(1):43–71, Mar. 1982. ISSN 0098-3500. doi: 10.1145/355984.355989. URL <http://doi.acm.org/10.1145/355984.355989>.
- S. K. Pakazad, M. S. Andersen, and A. Hansson. Distributed solutions for loosely coupled feasibility problems using proximal splitting methods. *Optimization Methods and Software*, 30(1):128–161, 2015. doi: 10.1080/10556788.2014.902056. URL <https://doi.org/10.1080/10556788.2014.902056>.

- N. Parikh and S. Boyd. Proximal algorithms. *Foundations and Trends® in Optimization*, 1(3):127–239, 2014. ISSN 2167-3888. doi: 10.1561/2400000003. URL <http://dx.doi.org/10.1561/2400000003>.
- P. Parpas. A multilevel proximal gradient algorithm for a class of composite optimization problems. *SIAM Journal on Scientific Computing*, 39(5):S681–S701, 2017. doi: 10.1137/16M1082299. URL <https://doi.org/10.1137/16M1082299>.
- B. Peters and F. J. Herrmann. Constraints versus penalties for edge-preserving full-waveform inversion. *The Leading Edge*, 36(1):94–100, 2017. doi: 10.1190/tle36010094.1. URL <http://dx.doi.org/10.1190/tle36010094.1>.
- B. Peters, B. R. Smithyman, and F. J. Herrmann. Projection methods and applications for seismic nonlinear inverse problems with multiple constraints. *GEOPHYSICS*, 0(ja):1–100, 2018. doi: 10.1190/geo2018-0192.1. URL <https://doi.org/10.1190/geo2018-0192.1>.
- G. Pratt, C. Shin, and G. Hicks. Gauss-Newton and full Newton methods in frequency-space seismic waveform inversion. *Geophysical Journal International*, 133(2):341–362, May 1998. ISSN 0956540X. doi: 10.1046/j.1365-246X.1998.00498.x. URL <http://doi.wiley.com/10.1046/j.1365-246X.1998.00498.x>.
- L. Ruthotto, E. Treister, and E. Haber. jinv—a flexible julia package for pde parameter estimation. *SIAM Journal on Scientific Computing*, 39(5):S702–S722, 2017. doi: 10.1137/16M1081063. URL <https://doi.org/10.1137/16M1081063>.
- Y. Saad. Krylov subspace methods on supercomputers. *SIAM Journal on Scientific and Statistical Computing*, 10(6):1200–1232, 1989. doi: 10.1137/0910073. URL <https://doi.org/10.1137/0910073>.
- M. Schmidt, E. Van Den Berg, M. P. Friedlander, and K. Murphy. Optimizing costly functions with simple constraints: A limited-memory projected quasi-newton algorithm. In *Proc. of Conf. on Artificial Intelligence and Statistics*, 2009.
- M. Schmidt, D. Kim, and S. Sra. *Projected Newton-type Methods in Machine Learning*, volume 35, chapter 11, pages 305–327. MIT Press, 04 2012.
- F. J. Serón, F. J. Sanz, M. Kindelán, and J. I. Badal. Finite-element method for elastic wave propagation. *Communications in Applied Numerical Methods*, 6(5):359–368, 1990. ISSN 1555-2047. doi: 10.1002/cnm.1630060505. URL <http://dx.doi.org/10.1002/cnm.1630060505>.
- B. Smithyman, B. Peters, and F. Herrmann. Constrained waveform inversion of colocated vsp and surface seismic data. In *77th EAGE Conference and Exhibition 2015*, 2015.
- C. Song, S. Yoon, and V. Pavlovic. Fast admm algorithm for distributed optimization with adaptive penalty. In *Proceedings of the Thirtieth AAAI Conference on Artificial Intelligence*, AAAI’16, pages 753–759. AAAI Press, 2016. URL <http://dl.acm.org/citation.cfm?id=3015812.3015924>.
- A. Tarantola. A strategy for nonlinear elastic inversion of seismic reflection data. *GEOPHYSICS*, 51(10):1893–1903, 1986. doi: 10.1190/1.1442046. URL <http://library.seg.org/doi/abs/10.1190/1.1442046>.
- R. J. Tibshirani. Dykstra's algorithm, admm, and coordinate descent: Connections, insights, and extensions. In I. Guyon, U. V. Luxburg, S. Bengio, H. Wallach, R. Fergus, S. Vishwanathan, and R. Garnett, editors, *Advances in Neural Information Processing Systems 30*, pages 517–528. Curran Associates, Inc., 2017.
- H. Trussell and M. Civanlar. The feasible solution in signal restoration. *IEEE Transactions on Acoustics, Speech, and Signal Processing*, 32(2):201–212, April 1984. ISSN 0096-3518. doi: 10.1109/TASSP.1984.1164297.

- M. Udell, K. Mohan, D. Zeng, J. Hong, S. Diamond, and S. Boyd. Convex optimization in julia. In *2014 First Workshop for High Performance Technical Computing in Dynamic Languages*, pages 18–28, Nov 2014. doi: 10.1109/HPTCDL.2014.5.
- E. van den Berg and M. P. Friedlander. Probing the pareto frontier for basis pursuit solutions. *SIAM Journal on Scientific Computing*, 31(2):890–912, 2009. doi: 10.1137/080714488. URL <https://doi.org/10.1137/080714488>.
- V. V. Vasin. Relationship of several variational methods for the approximate solution of ill-posed problems. *Mathematical notes of the Academy of Sciences of the USSR*, 7(3):161–165, Mar 1970. ISSN 1573-8876. doi: 10.1007/BF01093105. URL <https://doi.org/10.1007/BF01093105>.
- S. V. Venkatakrisnan, C. A. Bouman, and B. Wohlberg. Plug-and-play priors for model based reconstruction. In *2013 IEEE Global Conference on Signal and Information Processing*, pages 945–948, Dec 2013. doi: 10.1109/GlobalSIP.2013.6737048.
- J. Virieux and S. Operto. An overview of full-waveform inversion in exploration geophysics. *Geophysics*, 74(6):WCC1–WCC26, 2009. URL <http://dx.doi.org/10.1190/1.3238367>.
- Q. Wang, X. Zhang, Y. Zhang, and Q. Yi. Augem: Automatically generate high performance dense linear algebra kernels on x86 cpus. In *2013 SC - International Conference for High Performance Computing, Networking, Storage and Analysis (SC)*, pages 1–12, Nov 2013. doi: 10.1145/2503210.2503219.
- P. Witte, M. Louboutin, K. Lensink, M. Lange, N. Kukreja, F. Luporini, G. Gorman, and F. J. Herrmann. Full-waveform inversion, part 3: Optimization. *The Leading Edge*, 37(2):142–145, 2018. doi: 10.1190/tle37020142.1. URL <https://doi.org/10.1190/tle37020142.1>.
- M. Wytock, P.-W. Wang, and J. Zico Kolter. Convex programming with fast proximal and linear operators. *ArXiv e-prints*, Nov. 2015.
- Z. Xu, S. De, M. Figueiredo, C. Studer, and T. Goldstein. An empirical study of admm for nonconvex problems. In *NIPS workshop on nonconvex optimization*, 2016.
- Z. Xu, M. Figueiredo, and T. Goldstein. Adaptive ADMM with Spectral Penalty Parameter Selection. In A. Singh and J. Zhu, editors, *Proceedings of the 20th International Conference on Artificial Intelligence and Statistics*, volume 54 of *Proceedings of Machine Learning Research*, pages 718–727, Fort Lauderdale, FL, USA, 20–22 Apr 2017a. PMLR. URL <http://proceedings.mlr.press/v54/xu17a.html>.
- Z. Xu, M. A. T. Figueiredo, X. Yuan, C. Studer, and T. Goldstein. Adaptive relaxed admm: Convergence theory and practical implementation. In *The IEEE Conference on Computer Vision and Pattern Recognition (CVPR)*, July 2017b.
- Z. Xu, G. Taylor, H. Li, M. A. T. Figueiredo, X. Yuan, and T. Goldstein. Adaptive consensus ADMM for distributed optimization. In D. Precup and Y. W. Teh, editors, *Proceedings of the 34th International Conference on Machine Learning*, volume 70 of *Proceedings of Machine Learning Research*, pages 3841–3850, International Convention Centre, Sydney, Australia, 06–11 Aug 2017c. PMLR. URL <http://proceedings.mlr.press/v70/xu17c.html>.
- L. Ying, L. Demanet, and E. Candes. 3d discrete curvelet transform. In *Wavelets XI*, volume 5914, page 591413. International Society for Optics and Photonics, 2005.
- P. Yong, W. Liao, J. Huang, and Z. Li. Total variation regularization for seismic waveform inversion using an adaptive primal dual hybrid gradient method. *Inverse Problems*, 34(4):045006, 2018. URL <http://stacks.iop.org/0266-5611/34/i=4/a=045006>.

D. C. Youla and H. Webb. Image restoration by the method of convex projections: Part 1-theory. *IEEE Transactions on Medical Imaging*, 1(2):81–94, Oct 1982. ISSN 0278-0062. doi: 10.1109/TMI.1982.4307555.

K. Zhang, W. Zuo, S. Gu, and L. Zhang. Learning deep cnn denoiser prior for image restoration. In *2017 IEEE Conference on Computer Vision and Pattern Recognition (CVPR)*, pages 2808–2817, July 2017. doi: 10.1109/CVPR.2017.300.